Fig. 4

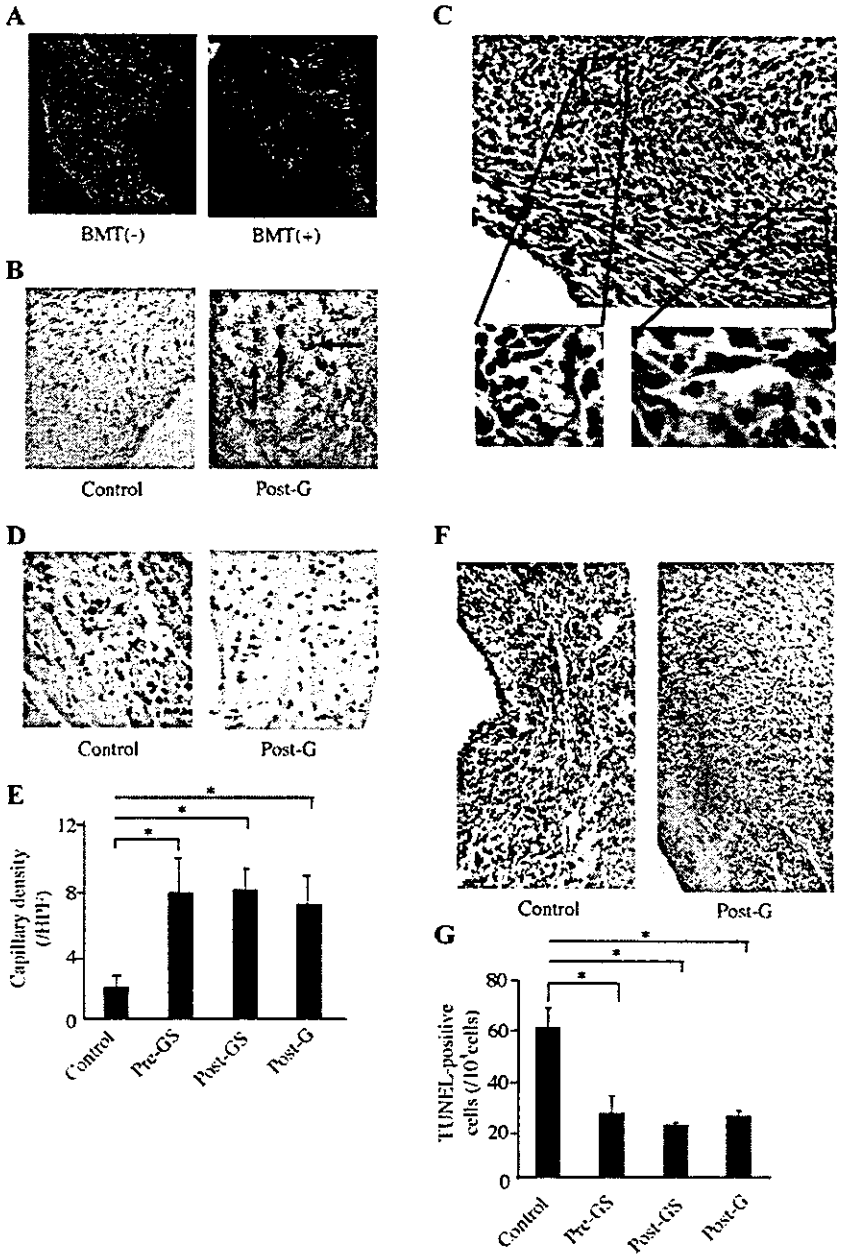

Figure 4. GFP-positive cells, capillary density and TUNEL-positive cells after MI. ***A***) Non-specific autofluorescence was recognized at the infarcted and border areas. BMT (–), infarcted heart of the mice without BM transplantation; BMT (+), infarcted heart of the mice whose BM was replaced with that of GFP mice. ***B***) Many GFP-positive cells (brown), which were mainly infiltrated blood cells, were recognized at the border area after MI in the three treatment groups with G-CSF. ***C***) GFP-positive cells were observed at capillary wall after MI in all the treatment groups. ***D***) The capillary density was examined by measuring PECAM-1-positive cells. ***E***) The density of capillaries at the border area was more increased in all the cytokine groups than in control group ($*P<0.05$). There was no significant difference of the capillary densities among the three treatment groups with G-CSF. ***F***) Apoptotic cells at Day 4 after MI. ***G***) The number of TUNEL-positive cells at the border area was less in all the treatment groups than in control group ($*P<0.05$). There was no significant difference in the number of TUNEL-positive cells among the three treatment groups.

Fig. 5

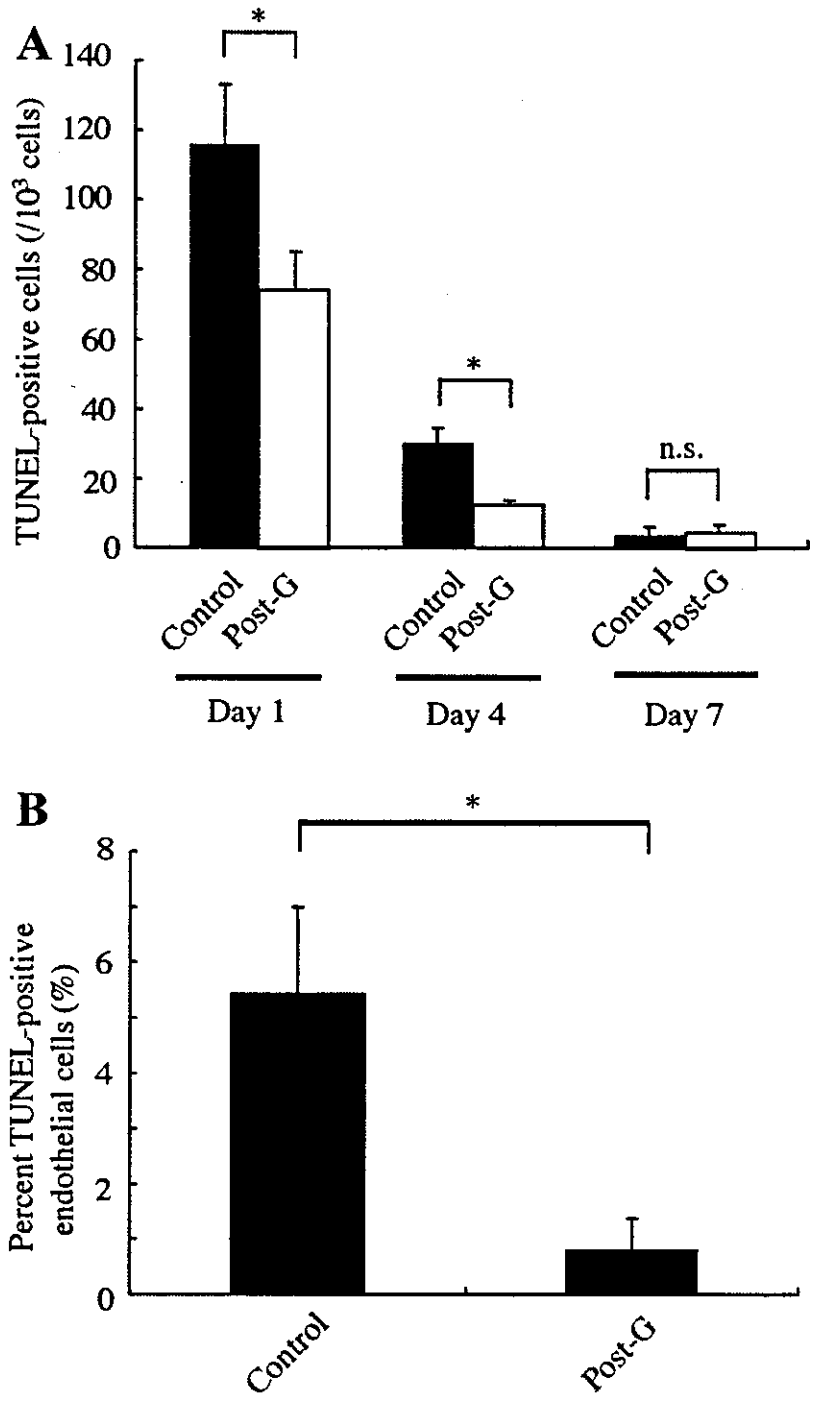

Figure 5. Apoptotic endothelial cell and non-endothelial cell death. *A*) At Day 1 and Day 4, the number of TUNEL-positive cells was significantly smallerin the Post-G group than in control group (*P<0.05). *B*) We checked double-immunohistochemical analysis to identify for the apoptotic endothelial cells at Day 1 after MI. The percentage of von Willebrand factor-positive cells in TUNEL-positive cells was significantly smaller in the Post-G group (*P<0.05).

Diabetologia (2004) 47:794–805
DOI 10.1007/s00125-004-1391-x

Diabetologia

Oxidative stress induces insulin resistance by activating the nuclear factor-κB pathway and disrupting normal subcellular distribution of phosphatidylinositol 3-kinase

T. Ogihara[1, 2] · T. Asano[1] · H. Katagiri[2] · H. Sakoda[3] · M. Anai[3] · N. Shojima[1] · H. Ono[3] · M. Fujishiro[1] · A. Kushiyama[1] · Y. Fukushima[1] · M. Kikuchi[3] · N. Noguchi[4] · H. Aburatani[4] · Y. Gotoh[5] · I. Komuro[6] · T. Fujita[1]

[1] Department of Internal Medicine, Graduate School of Medicine, University of Tokyo, Tokyo, Japan
[2] Division of Advanced Therapeutics for Metabolic Diseases, Center for Translational and Advanced Animal Research on Human Diseases, Tohoku University Graduate School of Medicine, Sendai, Japan
[3] The Institute for Adult Diseases, Asahi Life Foundation, Tokyo, Japan
[4] Research Center for Advanced Science and Technology, University of Tokyo, Tokyo, Japan
[5] Department of Molecular Biology, Institute of Molecular and Cellular Biosciences, University of Tokyo, Tokyo, Japan
[6] Department of Cardiovascular Science and Medicine, Chiba University Graduate School of Medicine, Chiba, Japan

Abstract

Aims/hypothesis. Oxidative stress is associated with diabetes, hypertension and atherosclerosis. Insulin resistance is implicated in the development of these disorders. We tested the hypothesis that oxidative stress induces insulin resistance in rats, and endeavoured to identify mechanisms linking the two.
Methods. Buthionine sulfoximine (BSO), an inhibitor of glutathione synthase, was administered to Sprague-Dawley rats and 3T3-L1 adipocytes. Glucose metabolism and insulin signalling both in vivo and in 3T3-L1 adipocytes were examined. In 3T3-L1 adipocytes, the effects of overexpression of a dominant negative mutant of inhibitory κB (IκB), one role of which is to block oxidative-stress-induced nuclear factor (NF)-κB activation, were investigated.
Results. In rats given BSO for 2 weeks, the plasma lipid hydroperoxide level doubled, indicating increased oxidative stress. A hyperinsulinaemic-euglycaemic clamp study and a glucose transport assay using isolated muscle and adipocytes revealed insulin resistance in BSO-treated rats. BSO treatment also impaired insulin-induced glucose uptake and GLUT4 translocation in 3T3-L1 adipocytes. In BSO-treated rat muscle, adipose tissue and 3T3-L1 adipocytes, insulin-induced IRS-1 phosphorylation in the low-density microsome (LDM) fraction was specifically decreased, while that in whole cell lysates was not altered, and subsequent translocation of phosphatidylinositol (PI) 3-kinase from the cytosol and the LDM fraction was disrupted. BSO-induced impairments of insulin action and insulin signalling were reversed by overexpressing the dominant negative mutant of IκB, thereby suppressing NF-κB activation.
Conclusions/interpretation. Oxidative stress induces insulin resistance by impairing IRS-1 phosphorylation and PI 3-kinase activation in the LDM fraction, and NF-κB activation is likely to be involved in this process.

Keywords Buthionine sulfoximine · Glutathione · Hyperinsulinaemic-euglycaemic clamp · Inhibitory κB · Insulin resistance · IRS · Nuclear factor-κB · Oxidative stress · Phosphatidylinositol 3-kinase

Received: 20 October 2003 / Accepted: 26 January 2004
Published online: 1 May 2004

T. Asano (✉)
Department of Internal Medicine, Graduate School of Medicine, University of Tokyo, Tokyo 113-8655, Japan
E-mail: asano-tky@umin.ac.jp
Tel.: +81-3-38153411 ext. 33133, Fax: +81-3-58031874

Present address:
T. Asano
Department of Physiological Chemistry and Metabolism, Graduate School of Medicine, University of Tokyo, Tokyo 113-8655, Japan

Introduction

Oxidative stress represents an imbalance between production of reactive oxygen species and the antioxidant defence system [1]. Oxidative stress is widely recognised as being associated with various disorders including diabetes, hypertension and atherosclerosis. In-

Abbreviations: BSO, buthionine sulfoximine · GMSA, gel mobility shift assay · IκB, inhibitory κB · IKK, IκB kinase · LDM, low-density microsome · NF-κB, nuclear factor-κB · PI, phosphatidylinositol

sulin resistance is a common feature of these disorders [2, 3]. Indeed, in diabetic people and in animal models of diabetes, the plasma free radical concentration is increased [4, 5] and antioxidant defences are diminished [6, 7]. It has also been suggested that antioxidant agents such as vitamin C [8] and E [9] improve insulin action in diabetic subjects.

Angiotensin II reportedly induces free radical production and increases plasma oxidative stress [10]. In our previous study, we showed continuous infusion of angiotensin II to induce insulin resistance with increased oxidative stress in rats, while the spin trap agent tempol [11], which works as a superoxide dismutase mimetic, decreases oxidative stress and improves insulin resistance in these rats [12]. A similar coexistence of oxidative stress and insulin resistance, as well as recovery with tempol administration was observed in adrenomedullin-deficient mice [13]. These previous reports strongly suggest a close relationship between oxidative stress and insulin resistance. Thus, we attempted to elucidate the molecular mechanisms underlying insulin resistance and oxidative stress.

In this study, to increase oxidative stress in vivo, we utilised a selective inhibitor of γ-glutamylcysteine synthetase, i.e. an inhibitor of glutathione synthase, buthionine sulfoximine (BSO). Glutathione is one of the major components of the antioxidant defence system, such that BSO administration increases oxidative stress by reducing the tissue glutathione level [14]. Although BSO does not have toxic effects in animals [14], BSO-treated rats were previously shown to exhibit glucose intolerance [15] and hypertension [16]. In the current study, we examined the effect of BSO treatment on insulin resistance in rats and 3T3-L1 adipocytes. We investigated the molecular mechanisms underlying BSO-induced insulin resistance, focusing on the subcellular distribution of phosphatidylinositol (PI) 3-kinase. Finally, we examined the involvement of the nuclear factor (NF)-κB pathway in BSO-induced insulin resistance and insulin signalling impairment.

Materials and methods

Materials. Affinity-purified antibodies against IRS-1 and GLUT4 were prepared as previously described [17]. Antibodies against phosphotyrosine, the p85 subunit of PI 3-kinase, and inhibitory κB (IκB) were purchased from Upstate Biotechnology (Milton Keynes, UK). TNF-α and buthionine-[S, R]-sulfoximine (BSO) were purchased from Sigma-Aldrich (St. Louis, Mo., USA).

Animals. Seven-week-old male Sprague-Dawley rats (Tokyo Experimental Animals, Tokyo, Japan) were fed a standard rodent diet with or without water containing 30 mmol/l BSO for 14 days [16]. The animal care was in accordance with the policies of the University of Tokyo, and the "Principles of laboratory animal care" (NIH publication no. 85-23, revised 1985) were followed.

Measurements. Cholesteryl ester hydroperoxides were analysed by HPLC, with 234 nm UV detection and post-column chemiluminescence detection on an LC-8 column (Supelco, 4×250 mm, 5-μm particles; Sigma-Aldrich) and methanol/tert-butyl alcohol (95/5 vol) as the eluent, as reported previously but with slight modification [18]. In brief, plasma was extracted with 10 volumes of methanol and 50 volumes of hexane. The hexane phase was removed, dried under N_2 gas and redissolved in an eluent for HPLC injection. Liver glutathione content was measured spectrophotometrically using a glutathione reductase recycling assay, as described previously [19].

Hyperinsulinaemic-euglycaemic clamp study. Rats fasted overnight were anaesthetised by intraperitoneal injection of pentobarbital sodium (60 mg/kg body weight) and the left jugular and femoral veins were catheterised for blood sampling and infusion respectively. Hyperinsulinaemic-euglycaemic clamp analysis was performed as described previously [17]. The glucose utilisation rate, hepatic glucose production and an estimate of muscle glucose uptake during the clamp (defined as the glucose metabolic index) were calculated as previously described [20].

Glucose uptake into isolated soleus muscle. Rats fasted overnight were anaesthetised and soleus muscles were dissected out and rapidly cut into 20–40 mg strips. The rats were then killed by intracardiac injection of pentobarbital. Isolated soleus muscle was incubated for 20 min with or without 1.44×10^{-8} mol/l human insulin (this concentration is equivalent to 2 mU/ml), as described previously [17]. 2-Deoxy glucose uptake into the isolated soleus muscle strips was measured using 2-deoxy-D-[^{3}H]glucose and [^{14}C]manitol as described previously [21].

Preparation of rat adipocytes and measurement of glucose uptake. Isolated rat adipocytes were prepared from epididymal adipose tissue harvested from fasted rats using the collagenase method [22], and 2-deoxy glucose uptake was then assayed as previously described [23].

Adenovirus-mediated gene transfer to 3T3-L1 adipocytes. 3T3-L1 fibroblasts were maintained in DMEM supplemented with 10% donor calf serum and differentiated into adipocytes as previously described [24]. The dominant negative mutant of IκB-α, in which serine residues 32 and 36 were substituted with alanine, was kindly provided by Dr R. Gaynor (University of Texas Southwestern Medical Center at Dallas, Tex., USA). To obtain recombinant adenovirus, pAdeno-X was ligated with cDNA encoding *Escherichia coli* lacZ and dominant negative IκB according to the manufacturer's instructions for the Adeno-X Expression System (Clontech, Palo Alto, Calif., USA). Infection of 3T3-L1 adipocytes with the adenovirus was carried out as described previously [25]. Recombinant adenoviruses were applied at a multiplicity of infection of approximately 200–300 pfu/cell and 3T3-L1 adipocytes infected with lacZ virus were used as a control.

Gel mobility shift assay. Nuclear protein extracts from 3T3-L1 adipocytes were prepared using NE-PER nuclear and cytoplasmic extraction reagents (Pierce Biotechnology, Rockford, Ill., USA) according to the manufacturer's instructions and used for gel mobility shift assay (GMSA). Briefly, 3T3-L1 adipocytes were homogenised in 1 ml of PBS and centrifuged for 10 min at 500 × *g* at 4 °C. After removing the supernatant, the pellet was resuspended in 500 μl of Cytoplasmic Extraction Reagent I buffer containing protease inhibitors (1 600 mol/l benzamidine, 0.3 mmol/l aprotinin, 4.2 mol/l leupeptin, 0.2 mol/l phenylmethylsulfonyl fluoride), and was incubated

on ice for 10 min. Then, 27.5 µl of Cytoplasmic Extraction Reagent II buffer were added to the sample, which was vortexed and centrifuged at 16 000 × *g* for 5 min. The resultant pellet was resuspended in 250 µl of NER buffer, vortexed every 10 minutes for 40 min and then centrifuged at 16 000 × *g* for 10 min. The supernatant containing nuclear proteins was stored at −80 °C. For the GMSA, 10 µg of nuclear proteins were incubated in binding buffer with 3.5 pmol of double-stranded DNA oligonucleotide containing an NF-κB consensus-binding sequence labelled with [^{32}P]-ATP using T4 polynucleotide kinase for 30 min at 37 °C. For supershift analyses, monoclonal antibody against NF-κB p65 was separately pre-incubated with nuclear extracts at 4 °C for 20 min in a total volume of 16 µl of binding buffer, followed by incubation with 8 µl of ^{32}P-labelled oligonucleotide probe with and without cold oligonucleotide probe at 4 °C for 20 min using a Nushift Kit (Geneka Biotechnology, Carlsbad, Calif., USA). Protein-DNA complexes were separated from the unbound DNA probe by electrophoresis through 5% polyacrylamide gels containing 1× Tris-glycine-EDTA buffer. The gel was dried and exposed to BAS2000 (Fujifilm, Tokyo, Japan).

Glucose uptake into 3T3-L1 adipocytes. 3T3-L1 adipocytes plated in 24-well culture dishes were serum starved for 3 h in DMEM containing 0.2% bovine serum albumin, after which they were incubated in Krebs–Ringer phosphate buffer for an additional 45 min, prior to incubation with or without 10^{-6} or 10^{-7} mol/l insulin for 15 min. The assay was initiated by adding 2-deoxy-D-[^{3}H]glucose (1.85×10^{7} Bq/sample, 0.1 mmol) and was terminated 4 min later by washing the cells once with ice-cold Krebs–Ringer phosphate buffer containing 0.3 mmol/l phloretin and then twice with ice-cold Krebs–Ringer phosphate buffer. The cells were then solubilised in 0.1% SDS, and the incorporated radioactivity was determined by scintillation counting [26].

Subcellular fractionation. 3T3-L1 adipocytes were serum starved for 3 h and incubated with or without 10^{-6} mol/l insulin for 15 min. Cells were fractionated as described previously [27]. Briefly, 3T3-L1 adipocytes were resuspended in HES buffer (255 mmol/l sucrose, 20 mmol/l HEPES [pH 7.4], 1 mmol/l EDTA), homogenised and subjected to differential centrifugation. The supernatants from the following spins were serially removed and pelleted in a Ti70 rotor as follows: 19 000 × *g* (20 min), 41 000 × *g* (20 min) and 180 000 × *g* (75 min). The first 19 000 × *g* pellet was resuspended, loaded onto a sucrose cushion (1.12 mol/l sucrose, 20 mmol/l HEPES [pH 7.4], 1 mmol/l EDTA) and isolated from the interface yielding the plasma membrane fraction as the pellet of a 41 000 × *g* spin (20 min). The last 180 000 × *g* pellet corresponded to the low-density microsome (LDM) fraction. Subcellular fractionation and measurement of GLUT4 translocation in isolated skeletal muscle and adipocytes from rats were described previously [12]. After resuspension of the pellets in solubilisation buffer, 20 µg of each fraction were loaded for western blotting. Proteins in the plasma membrane and LDM fractions were separated by SDS-PAGE, transferred to a polyvinylidene fluoride membrane, immunoblotted with anti-GLUT4, anti-IRS-1 or anti-p85 antibodies, and reacted with enhanced chemiluminescence reagent (Amersham Biosciences, Uppsala, Sweden) or subject to immunoprecipitation and PI 3-kinase assay of the immunoprecipitates as previously described [17].

Immunoprecipitation and immunoblotting. In rat experiments, rats fasted overnight were anaesthetised, and within 10–15 min the abdominal cavity was opened, the portal vein exposed, and 16 ml/kg body weight of normal saline (0.9% NaCl), with or without 10^{-5} mol/l human insulin, were injected. After 60 s, hindlimb muscles were removed and immediately homogenised as described previously [28]. In 3T3-L1 experiments, 3T3-L1 adipocytes were serum-starved for 18 h, pre-incubated with or without 80 µmol/l BSO for 18 h, then stimulated with or without 10^{-6} mol/l insulin for 15 min. The cells were then washed and lysed with lysis buffer as described previously [29]. After centrifugation, the resultant supernatants were used for immunoprecipitation or immunoblotting as described previously [28]. Proteins were visualised with enhanced chemiluminescence and band intensities were quantified with a Molecular Imager GS-525 using Imaging Screen-CH (Bio-Rad Laboratories, Hercules, Calif., USA). In some experiments, 3T3-L1 cells were incubated with 5.8 pmol/l (equivalent to 10 ng/dl) TNF-α or 80 µmol/l BSO for 18 h, lysed and immunoblotted with anti-IκB antibody.

Phosphatidylinositol 3-kinase activity. After preparing tissue samples as above, IRS-1 was immunoprecipitated, and PI 3-kinase activity in the immunoprecipitates was assayed as previously described [17].

Statistical analysis. Data are expressed as means ± SE. Comparisons between the two groups were made using unpaired *t* tests. We considered *p* values of less than 0.05 to be statistically significant.

Results

Characterisation of rats studied. Although food intakes were similar in the two groups, the BSO-treated rats had lower body weights than control rats (Table 1). Individual water consumptions did not differ between the two. Systolic and diastolic blood pressures were similar in the two groups of rats. Fasting blood glucose and plasma insulin levels in BSO rats were also similar to those of control rats. Although fasting insulin levels were not elevated in BSO-treated rats as compared with those of controls, we found that

Table 1. Characterisation of BSO-treated rats

	Control	BSO
Body weight (g)	320.0±8.7	284±4.1*
Food intake (g/day)	20.2±2.4	21.2±2.3
Water intake (ml/day)	38.2±1.8	36.8±3.2
Systolic BP (mm Hg)	113.5±4.4	120.7±3.9
Diastolic BP (mm Hg)	83.4±4.4	87.8±1.4
Fasting blood glucose (mmol/l)	6.12±0.32	6.32±0.24
Randomly fed blood glucose (mmol/l)	8.37±0.24	8.44±0.17
Fasting plasma insulin (pmol/l)	109±16	112±3
Randomly fed plasma insulin (pmol/l)	188±17	367±3*
Glutathione content of liver (µmol/g tissue)	3.2±0.3	1.1±0.4*
Plasma cholesteryl ester hydroperoxide (mmol/l)	1.38±0.3	2.72±0.3*

Data are means ± SE; rats in each group, n=6; * p<0.05 compared with controls

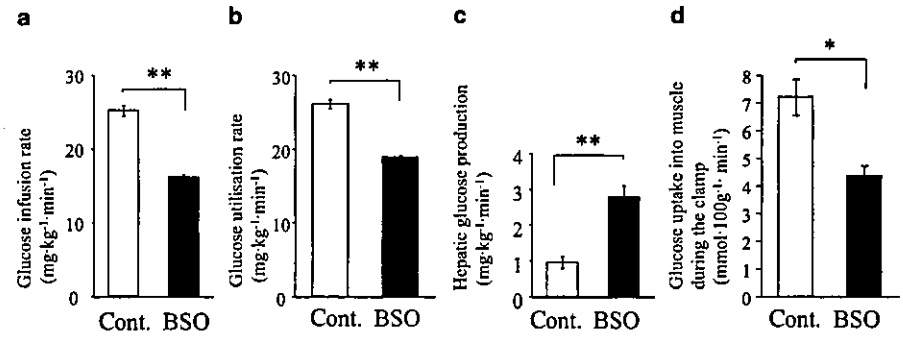

Fig. 1. A hyperinsulinaemic-euglycaemic clamp study. Rats were anaesthetised by intraperitoneal injection of pentobarbital sodium and the left jugular and femoral veins were catheterised for blood sampling and infusion respectively. Hyperinsulinaemic-euglycaemic clamp analysis was performed as described previously [17]. The glucose infusion rate (**a**), glucose utilisation rate (**b**), hepatic glucose production (**c**) and muscle glucose uptake during the clamp (defined as the glucose metabolic index; **d**) were estimated from hyperinsulinaemic-euglycaemic clamp data. * $p<0.05$, ** $p<0.01$ compared with the control. Bars represent the means ± SE of results from four to five rats. Cont. indicates control Sprague-Dawley rats. BSO indicates rats fed a standard rodent diet with water containing 30 mmol/l BSO for 12 days

among well-fed animals, insulin levels in BSO-treated rats were significantly higher than those in controls. To determine the effect of BSO as a glutathione synthase inhibitor, hepatic glutathione content was measured, because glutathione is most abundant in the liver. The glutathione level was significantly lower, by 34%, in the livers of BSO-treated rats than in those of controls. The cholesteryl ester hydroperoxide level in BSO-treated rat plasma was double that in control rats, suggesting that oxidative stress is increased in BSO-treated rats.

Hyperinsulinaemic-euglycaemic clamp study. Whole-body insulin sensitivity was evaluated using a hyperinsulinaemic-euglycaemic clamp technique. Compared with controls, the glucose infusion rate was decreased by 36.2% and the glucose utilisation rate by 27.6% during submaximal insulin infusion in BSO-treated rats (Figs. 1a, b). In addition, hepatic glucose production was increased by 29.3% in BSO-treated rats, suggesting impairment of the ability of insulin to suppress hepatic glucose production (Fig. 1c). Glucose uptake into skeletal muscle during the clamp was decreased by 39.4% in BSO-treated rats (Fig. 1d). These results suggest that BSO treatment induces insulin resistance both systemically and in skeletal muscle and liver.

Insulin-induced glucose uptake and GLUT4 translocation in BSO-treated rat skeletal muscle and adipocytes. In BSO-treated rats, insulin-induced glucose uptakes into isolated soleus muscle and adipocytes were reduced by 21.4% and 47.8% respectively as compared with the control levels (Figs. 2a, c). Subsequent western blot analysis showed the GLUT4 contents of skeletal muscle and adipocytes to be similar in the two groups (Figs. 2b, d, upper panels), indicating that the impairment of insulin-induced glucose uptake in these tissues from BSO-treated rats was not due to reduced expression of GLUT4 proteins. However, insulin-induced GLUT4 translocation, as assessed by the appearance of GLUT4 in the plasma membrane fraction of skeletal muscle and adipose tissue, was decreased in BSO-treated rats (Figs. 2b, d, lower panels). Microscopic analysis revealed adipocytes from BSO-treated rats to be small, which is consistent with the low body weights of these rats (Fig. 2e), suggesting that insulin resistance in BSO-treated rats is not attributable to adipocyte enlargement.

Impairment of insulin signalling in BSO-treated rat skeletal muscle and adipocytes. Next, we investigated insulin-induced tyrosine phosphorylation of IRS-1, association of PI 3-kinase with IRS-1, and PI 3-kinase activation in skeletal muscle and adipose tissue in vivo by injecting insulin through the portal vein of anaesthetised rats. Protein amount and insulin-induced tyrosine phosphorylation of IRS-1 in skeletal muscle (whole tissue lysates) from BSO-treated rats were similar to those in controls (Fig. 3a, upper panels). Because the insulin signalling in the LDM fraction has been implicated in several insulin actions including insulin-induced glucose uptake [30, 31], we carried out subcellular fractionation studies of skeletal muscles from these rats. Subcellular fractionation data showed insulin-induced tyrosine phosphorylation of IRS-1 in the LDM fraction to be significantly decreased in BSO-treated rats as compared with controls, although the IRS-1 protein amount in this fraction was unchanged (Fig. 3a, upper panels). In the cytosol, the amount of IRS-1 and insulin-induced phosphorylation were similar in BSO-treated and control rat muscles (Fig. 3a, upper panels). Next, we investigated the amount of the p85 subunit for PI 3-kinase protein in whole tissue lysates, the LDM fraction and the cytosol (Fig. 3a, middle panels). The amounts of p85 protein were similar in whole tissue

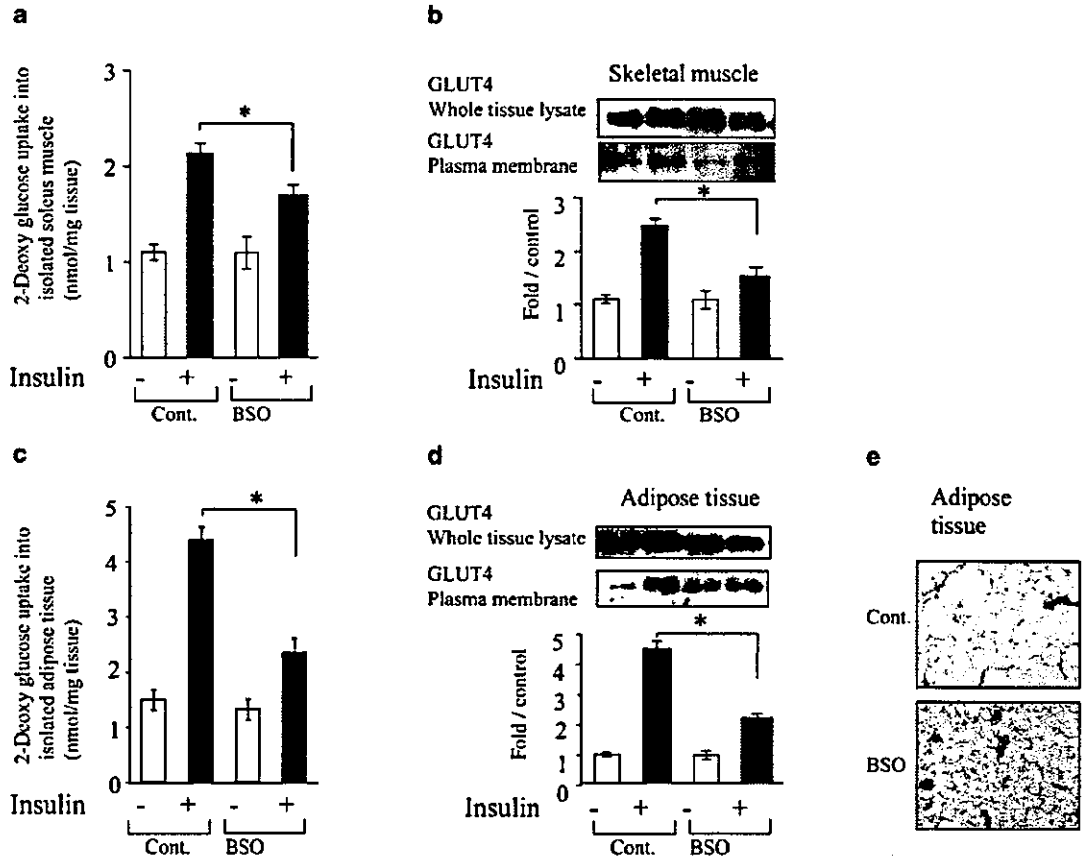

Fig. 2. Insulin resistance in isolated skeletal muscle and adipose tissue in BSO-treated rats. **a.** 2-Deoxy-glucose uptakes into isolated soleus muscle and adipose tissue (**c**). Isolated rat soleus muscle was incubated for 20 min with or without 1.44×10^{-8} mol/l human insulin (this concentration is equivalent to 2 mU/ml) as described previously [17]. 2-Deoxy-D-[1-^{3}H]glucose uptake into the isolated soleus muscle strips was measured as described previously [21]. Isolated rat adipocytes were prepared from epididymal adipose tissue harvested from fasted rats using the collagenase method [22], and 2-deoxy glucose uptake was then assayed as previously described [23]. **b, d.** GLUT4 protein amount in whole tissue lysates (upper panels), the plasma membrane fraction (lower panels) of skeletal muscle (**b**) and adipose tissue (**d**) under basal or insulin-stimulated conditions. Subcellular fractionation and measurement of GLUT4 translocation of isolated skeletal muscle and adipocytes from rats were described previously [12]. Whole tissue lysates and plasma membrane fractions were subjected to SDS-PAGE followed by immunoblotting with anti-GLUT4 antibody. The data are representative of three independent experiments. Bars depict means ± SE of the results from four to six samples. * $p<0.05$ compared with the control under the insulin-stimulated conditions. **d.** Haematoxylin and eosin stained adipose tissues from control and BSO-treated rats are shown. Cont. indicates control Sprague-Dawley rats. BSO indicates rats fed a standard rodent diet with water containing 30 mmol/l BSO for 12 days

lysates before and after insulin stimulation. However, insulin stimulation induced a p85 increase in the LDM fraction and a decrease in the cytosol, suggesting that insulin stimulates p85 translocation from the cytosol to the LDM fraction. This insulin-induced translocation of p85 was disrupted in BSO-treated rats. Insulin-induced increases in IRS-1-associated p85 protein and PI 3-kinase activity did not differ significantly between whole tissue lysates and the cytosol in either BSO-treated or control rat muscle (Fig. 3a, lower panels). However, both were significantly decreased in the LDM fraction of BSO-treated rats as compared with the controls. We obtained essentially the same results in the adipose tissue of these rats (Fig. 3b). In addition, we confirmed that insulin-induced tyrosine phosphorylation of the insulin receptor and IRS-2, as well as Ser-473 phosphorylation of Akt, in the whole tissue lysates of skeletal muscle and adipose tissue does not differ between BSO-treated and control rats (data not shown). Thus, early insulin-signalling steps were shown to be impaired specifically in the LDM fraction, but not in whole tissue lysates of skeletal muscle and adipose tissue from BSO-treated rats.

Insulin action and insulin signalling in BSO-treated 3T3-L1 adipocytes. To further investigate the impaired step in BSO-induced insulin resistance, 3T3-L1

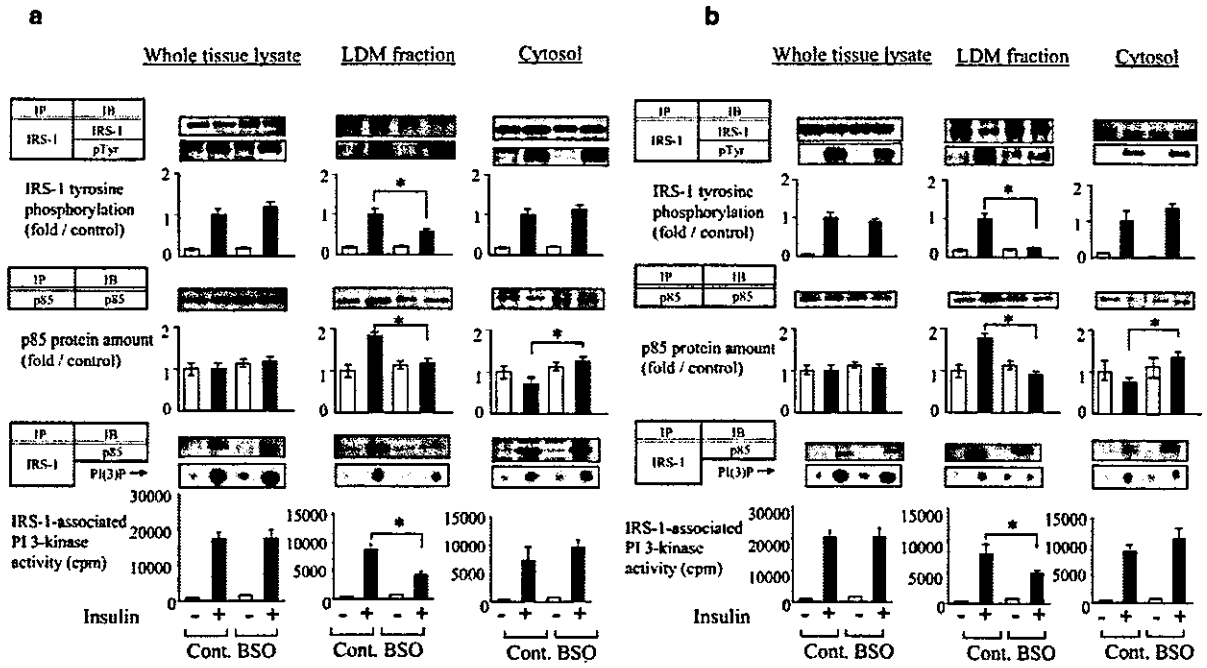

Fig. 3. Insulin signalling in skeletal muscle (**a**) and adipose tissue (**b**) from BSO-treated rats. Rats were anaesthetised, the portal vein exposed, and 16 ml/kg body weight of normal saline, with or without 10^{-5} mol/l human insulin, were injected. After 60 s, hindlimb muscles and epididymal fat were removed and immediately homogenised as described previously [28]. After centrifugation, the resultant supernatants were employed for immunoprecipitation or immunoblotting using the indicated antibodies as described previously [28]. Proteins were visualised with enhanced chemiluminescence and band intensities were quantified with a Molecular Imager GS-525 using Imaging Screen-CH (Bio-Rad). Bars depict means ± SE of the quantitated tyrosine phosphorylation bands, independently obtained in triplicate. Representative spots of PI(3)P are shown in the lower panels and bars depict means ± SE of PI 3-kinase activity measured in three independent assays. * $p<0.05$ compared with the control under the insulin-stimulated condition. IP, immunoprecipitation; IB, immunoblotting; pTyr, phosphotyrosine

adipocytes were incubated with 80 μmol/l BSO for 18 h [32]. It was reported that BSO treatment of adipocytes markedly decreases cellular glutathione levels and increases reactive oxygen species [15, 32]. Incubation with BSO did not affect the morphology or the viability of 3T3-L1 adipocytes (data not shown). Insulin-induced glucose uptake into 3T3-L1 adipocytes was decreased by 42.5% in BSO-treated cells (Fig. 4a). In these cells, insulin-induced GLUT4 translocation to the plasma membrane was impaired (Fig. 4b). Next, we determined insulin-induced IRS-1 phosphorylation and PI 3-kinase activation in whole cell lysates, the LDM fraction and the cytosol. As in rats, protein levels and insulin-induced tyrosine phosphorylations of IRS-1 and IRS-1-associated PI 3-kinase were unaffected by BSO treatment (Fig. 4c, upper panel). In control cells and in BSO-treated cells, p85 protein levels did not differ before versus after insulin stimulation. Next, we examined IRS-1 tyrosine phosphorylation and IRS-1 associated PI 3-kinase activity in the LDM fraction and the cytosol. While IRS-1 protein levels did not change after incubation with BSO, insulin-induced IRS-1 tyrosine phosphorylation in the LDM fraction was suppressed by BSO treatment (Fig. 4c, middle panel). The amount of p85 protein was increased in the LDM fraction and decreased in the cytosol after insulin stimulation, indicating that insulin induces p85 translocation from the cytosol to the LDM fraction in control cells. However, the p85 increase in the LDM fraction was clearly disrupted in BSO-treated cells (Fig. 4c, middle panel). In parallel, insulin-stimulation increased IRS-1-associated p85 protein levels and PI 3-kinase activity in the LDM fraction of control but not BSO-treated cells. Thus, BSO treatment disrupts insulin-induced IRS-1 phosphorylation in the LDM fraction and the subcellular redistribution of PI 3-kinase in 3T3-L1 adipocytes.

Inhibition of NF-κB activation improves BSO-induced insulin resistance. It is widely known that one potential target of oxidative stress is the activation of transcription factor NF-κB [33]. Oxidative stress and inflammatory cytokine stimulation reportedly activate upper kinase IκB kinase (IKK) which phosphorylates serine residues of IκB. The phosphorylated IκB is then subject to degradation, leading to translocation of NF-κB to the nucleus [34]. To investigate the role of NF-κB cascade activation in BSO-induced insulin re-

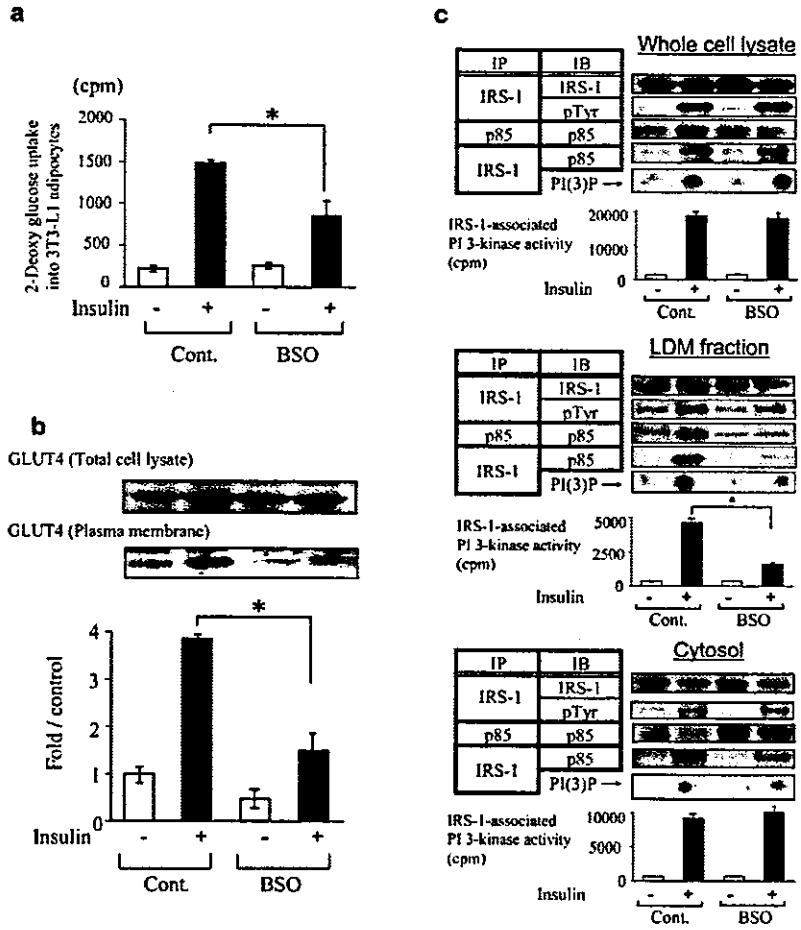

Fig. 4. Effects of BSO treatment on insulin action and insulin signalling in 3T3-L1 adipocytes. **a.** Insulin-induced 2-deoxy glucose uptake into 3T3-L1 adipocytes. 3T3-L1 adipocytes were serum-starved for 18 h, pre-incubated with or without 80 μmol/l BSO for 18 h, then incubated with or without 10^{-6} mol/l insulin for 15 min. 2-Deoxy glucose uptake was measured as described in Materials and methods. Bars depict means ± SE of results obtained independently in triplicate. * $p<0.05$ compared with the insulin-stimulated control. **b.** Recruitment of GLUT4 to the plasma membrane in 3T3-L1 adipocytes with or without BSO pretreatment. 3T3-L1 adipocytes were serum-starved for 18 h, pre-incubated with or without 80 μmol/l BSO for 18 h, then stimulated with or without 10^{-6} mol/l insulin for 15 min. Cells were fractionated as described previously [27]. The cell lysates and plasma membrane fraction were immunoblotted with anti-GLUT4 antibody. Representative immunoblots using anti-GLUT4 antibody are shown. Bars depict means ± SE of the quantitated bands of the plasma membrane fraction, independently obtained in triplicate. **c.** IRS-1 phosphorylation and IRS-1-associated PI 3-kinase in whole cell lysates (upper panels), the LDM fraction (middle panels) and the cytosol (lower panels) in 3T3-L1. 3T3-L1 adipocytes were serum-starved for 18 h, pre-incubated with or without 80 μmol/l BSO for 18 h, then stimulated with or without 10^{-6} mol/l insulin for 15 min. Subcellular fractionation was performed as described in Materials and methods. The whole cell lysates and fractions were used for immunoprecipitation, immunoblotting and PI 3-kinase assay as described previously [28]. Proteins were visualised with enhanced chemiluminescence and band intensities were quantified with a Molecular Imager GS-525. Representative immunoblots are shown in the upper and middle panels and representative spots of PI(3)P, independently obtained in triplicate, are shown in the lower panel. Bars depict means ± SE of the quantitated spots of PI(3)P, indicating IRS-1-associated PI 3-kinase activity, independently obtained in triplicate. Cont., control 3T3-L1 adipocytes; BSO, pre-treated with 80 μmol/l BSO for 18 h. * $p<0.05$ compared with the control under the insulin-stimulated condition

sistance, we overexpressed the dominant negative mutant of IκB in 3T3-L1 adipocytes using adenovirus. This mutant, characterised by the substitution of two serine phosphorylation sites to alanine, is resistant to degradation and inhibits NF-κB-induced transcription. In 3T3-L1 adipocytes, endogenous IκB was degraded by 5.8 pmol/l (equivalent to 10 ng/dl) of TNF-α or 80 μmol/l BSO pre-incubation for 18 h (Fig. 5a). However, the dominant negative IκB, overexpressed using adenovirus, was not degraded by these treat-

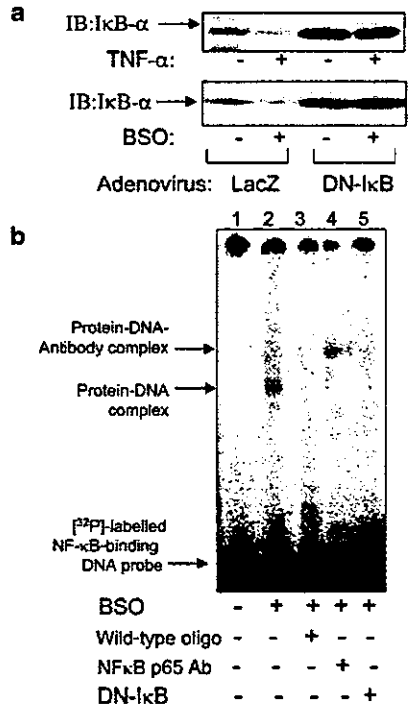

Fig. 5. Dominant negative mutant of IκB. **a.** Immunoblot of 3T3-L1 adipocytes overexpressing LacZ (control) and dominant negative mutant of I-κB adenoviruses. Representative immunoblots with anti-IκBα antibody of the cells incubated with 5.8 pmol/l (equivalent to 10 ng/ml) TNF-α and 80 μmol/l BSO for 18 h are shown in the upper and lower panels respectively. **b.** Gel mobility shift assay (GMSA). 3T3-L1 adipocytes were incubated with (lanes 2–5) or without (lane 1) 80 μmol/l BSO for 18 h. Dominant negative IκB was overexpressed in 3T3-L1 adipocytes (lane 5). Nuclear protein extracts from 3T3-L1 adipocytes were prepared as described in Materials and methods. For the GMSA, 10 μg of nuclear proteins were incubated in binding buffer with 3.5 pmol of double-stranded DNA oligonucleotide containing an NF-κB consensus binding sequence labelled with [^{32}P]-ATP using T4 polynucleotide kinase, for 30 min at 37 °C. For supershift analyses, monoclonal antibody against NF-κB p65 (NF-κB p65 Ab, lane 4) was separately pre-incubated with nuclear extracts at 4 °C for 20 min in a total volume of 16 μl of binding buffer, followed by incubation with 8 μl of ^{32}P-labelled oligonucleotide probe with and without a cold oligonucleotide probe (wild-type oligo, lane 3) at 4 °C for 20 min using a Nushift Kit (Geneka Biotechnology). Protein-DNA complexes were separated from the unbound DNA probe by electrophoresis through 5% polyacrylamide gels containing 1× Tris-glycine-EDTA buffer. The gel was dried and exposed to BAS2000 (Fujifilm, Tokyo, Japan). DN, dominant negative; IB, immunoblotting

ments (Fig. 5a). To investigate whether NF-κB binds to regulatory DNA elements, GMSA was performed using nuclear extracts of 3T3-L1 adipocytes. GMSA revealed nuclear protein extracts from BSO-treated 3T3-L1 adipocytes to contain activated NF-κB (Fig. 5b, lanes 1 and 2). The band shift was inhibited by unlabelled oligonucleotide corresponding to a DNA-binding sequence (Fig. 5b, lane 3). In BSO-treated cells, the NF-κB-oligonucleotide complex underwent a supershift in the presence of antibodies against the p65 subunit of NF-κB, indicating that binding to the oligonucleotide is NF-κB-specific (Fig. 5b, lane 4). In 3T3-L1 adipocytes overexpressing the dominant negative IκB, the band shift was also inhibited (Fig. 5b, lane 5). These results suggest that BSO treatment induces NF-κB translocation and that the dominant negative IκB blocks NF-κB pathway activation.

We next examined the effect of the dominant negative IκB on BSO-induced insulin resistance. Insulin-induced glucose uptake was decreased by BSO treatment, while dominant negative IκB overexpression reversed this decrease (Fig. 6a). Reduction of insulin-induced GLUT4 translocation by BSO administration was also reversed by overexpression of the dominant negative IκB (Fig. 6b). BSO treatment decreased insulin-induced IRS-1 phosphorylation and IRS-1-associated p85 and PI 3-kinase activity in the LDM fraction (Fig. 6c, lower panels), but not in whole cell lysates (Fig. 6c, upper panels). However, overexpression of the dominant negative IκB reversed the BSO-induced decreases in IRS-1 phosphorylation and IRS-1-associated p85 and PI 3-kinase activity in the LDM fraction. These results suggest that oxidative stress induces insulin resistance by impairing the normal subcellular distribution of PI 3-kinase, and that the NF-κB pathway is involved in this process.

Discussion

In this study we employed BSO, a glutathione synthase inhibitor, to induce oxidative stress in rats and in 3T3-L1 adipocytes. BSO specifically inhibits the first step of glutathione synthesis and decreases glutathione, an important component of the antioxidant defence system [14]. In fact, we confirmed a decreased hepatic glutathione content and an increased plasma lipid hydroperoxide level, indicating increased oxidative stress in BSO-treated rats. Body weight was lower in BSO-treated rats than in controls, which is consistent with a previous report [35]. BSO-treated rats were apparently insulin-resistant, as demonstrated by a hyperinsulinaemic-euglycaemic clamp study and glucose transport assay using isolated skeletal muscle and adipocytes. These results strongly support the hypothesis that increased oxidative stress can lead to insulin resistance in vivo. Although fasting insulin levels were not elevated in BSO-treated rats as compared with controls, we found that among well-fed animals, insulin levels were significantly higher in BSO-treated rats than in controls. Data from the euglycaemic-hyperinsulinaemic clamp study, along with the observed glucose uptake into isolated tissues and insulin levels in well-fed animals, support the

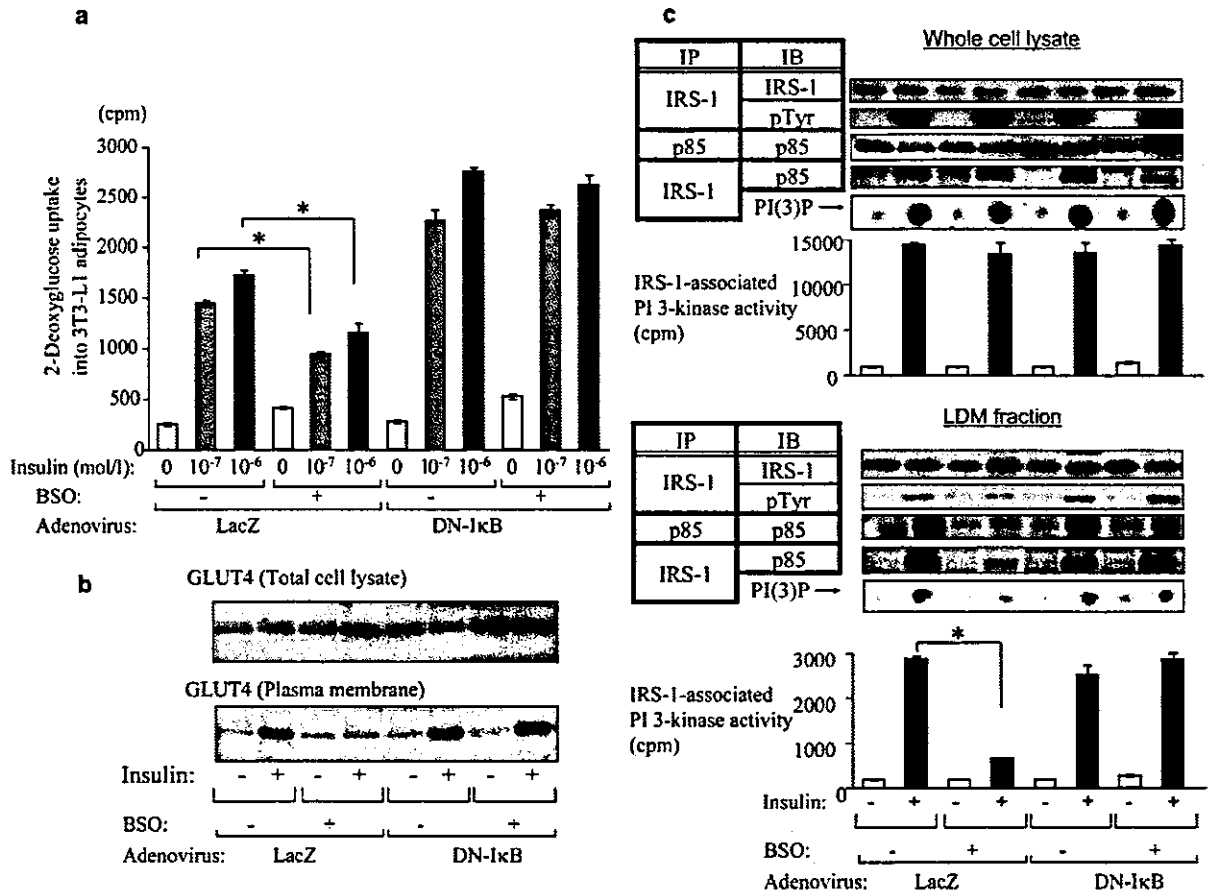

Fig. 6. Effect of dominant negative mutant of IκB on insulin action and insulin signalling in BSO-treated 3T3-L1 adipocytes. **a.** Insulin-induced 2-deoxy glucose uptake into 3T3-L1 adipocytes. Cells overexpressing LacZ (control) and the dominant negative (DN)-IκB adenovirus with or without 80 μmol/l BSO for 18 h were stimulated were stimulated with 0, 10^{-7} or 10^{-6} mol/l insulin for 15 min. Glucose uptake into 3T3-L1 adipocytes was assayed as described in Materials and methods. Bars depict means ± SE of results obtained independently in triplicate. ** $p<0.05$ compared to insulin-stimulated (10^{-7} and 10^{-6} mol/l respectively) control (non BSO-treated) cells. **b.** Recruitment of GLUT4 to the plasma membrane in 3T3-L1 adipocytes overexpressing LacZ and DN-IκB adenovirus with or without BSO pretreatment. The cell lysates and plasma membrane fraction were immunoblotted with anti-GLUT4 antibody. **c.** IRS-1 tyrosine phosphorylation, p85 protein amount and IRS-1-associated PI 3-kinase in whole cell lysates (upper panels) and the LDM fraction (lower panels) of 3T3-L1 adipocytes overexpressing LacZ and DN-IκB adenovirus with or without BSO pretreatment. 3T3-L1 adipocytes were serum-starved for 18 h, pre-incubated with or without 80 μmol/l BSO for 18 h, then stimulated with or without 10^{-6} mol/l insulin for 15 min. Representative immunoblots and representative spots of PI(3)P, independently obtained in triplicate, are shown and bars depict means ± SE of PI 3-kinase activity measured in three independent assays. * $p<0.05$ compared with insulin-stimulated control (non BSO-treated) cells. IB, immunoblotting; IP, immunoprecipitation

conclusion that BSO-treated rats are insulin-resistant. In our experiments, we did not observe the occurrence of overt diabetes with BSO administration, suggesting that this insulin resistance is relatively mild.

A previous report showed no significant difference between BSO-injected rats and controls in terms of insulin-stimulated glucose transport into skeletal muscle [15]. The results of their study contradict our present data demonstrating BSO-induced insulin resistance. We speculate that these different results are attributable to the doses of BSO administered. According to our water consumption data, intake of BSO in BSO-treated rats was approximately 3.5 mmol·kg^{-1} body weight·day^{-1} in the current study. This is a rather high dose compared with the previous report (2 mmol·kg^{-1} body weight·day^{-1}) [15]. Also, the extent of the glutathione decrease was greater in our experiment than in the previous one. In addition, because the previous study did not employ the hyperinsulinaemic-euglycaemic clamp method [15], we believe our picture of insulin resistance in BSO-treated rats to be more accurate.

Insulin-induced IRS phosphorylation and PI 3-kinase activation constitute a critical step in insulin actions such as GLUT4 translocation and glucose uptake [36]. Most insulin-resistant models have been shown

to have impaired insulin-induced PI 3-kinase activation [28, 37, 38]. However, in the BSO-treated rats used in the current study, neither insulin-induced IRS tyrosine phosphorylation nor PI 3-kinase activation in whole tissue lysates of skeletal muscle and adipose tissue were impaired, despite the presence of insulin resistance. In addition, BSO treatment markedly impaired insulin-induced glucose uptake into 3T3-L1 adipocytes and GLUT4 translocation, while insulin-induced IRS-1 tyrosine phosphorylation and IRS-1-associated PI 3-kinase activation were unchanged in whole cell lysates of BSO-treated 3T3-L1 adipocytes. A previous report showed H_2O_2 exposure of 3T3-L1 adipocytes to inhibit insulin-induced glucose uptake, while having no effects on IRS-1 phosphorylation and PI 3-kinase activation [39]. Furthermore, we previously reported chronically angiotensin-II-infused rats, in which plasma lipid hydroperoxide levels were increased, to be highly insulin-resistant, although insulin-induced IRS-1 phosphorylation and PI 3-kinase activation in skeletal muscle and adipose tissue were not impaired [12]. Thus, insulin resistance with normal insulin-induced PI 3-kinase activation in the whole cell may be a common feature in the models with increased oxidative stress.

Regarding the molecular mechanism of this type of insulin resistance, we consider it necessary to examine the possibility of abnormalities in the subcellular distribution of PI 3-kinase. This is based on several reports showing IRS-1 phosphorylation and PI 3-kinase activation specifically in the LDM fraction, though not in whole cell lysates, to be important for insulin action [30, 31]. We speculate that the insulin-induced increase in IRS-1 phosphorylation in the LDM fraction leads to recruitment of the p85 subunit for PI 3-kinase to that fraction. Previous reports have shown that H_2O_2 exposure reduces IRS-1 tyrosine phosphorylation and PI 3-kinase activation in the LDM fraction in 3T3-L1 adipocytes [39, 40]. In the current study, insulin-induced IRS-1 tyrosine phosphorylation in the LDM fraction was demonstrated to be significantly decreased in both BSO-treated rat muscle and adipose tissues and in BSO-treated 3T3-L1 cells. We showed clearly that insulin induces p85 translocation from the cytosol to the LDM fraction in rat muscle, adipose tissue and 3T3-L1 cells and that BSO treatment disrupts this process. Taking our results and those of previous reports together, we consider this disruption of the normal subcellular redistribution of PI 3-kinase to be one of the important mechanisms underlying oxidative-stress-induced insulin resistance.

The activation of transcription factor NF-κB has been shown to be a target of oxidative stress [33]. For example, direct exposure to oxidants such as H_2O_2 activates NF-κB [41], while NF-κB activation can be inhibited by addition of antioxidants such as a vitamin E derivative [42] and lipoic acid [43]. To clarify the contribution of NF-κB cascade activation to oxidative-stress-induced insulin resistance, we utilised the dominant negative IκB. This mutant is a degradation-resistant form of IκB that prevents NF-κB from translocating into the nucleus and is widely used to block cytokine-induced NF-κB activation [44]. Indeed, we confirmed that this mutant is not degraded by TNF-α and that BSO stimulation blocks NF-κB from translocating into the nucleus. Blocking the NF-κB cascade by overexpressing dominant negative IκB had a preventive effect against the decrease in insulin-induced glucose uptake and GLUT4 translocation caused by BSO treatment in 3T3-L1 adipocytes. We observed higher glucose uptake in dominant negative IκB-overexpressing cells than in LacZ control cells. We suggest a possible explanation: dominant negative IκB inhibits the effects of a small amount of inflammatory cytokines secreted by adipocytes. In addition, BSO-induced decreases in IRS-1 tyrosine phosphorylation in the LDM fraction and recruitment of PI 3-kinase to that fraction were also normalised. These results suggest that NF-κB activation is involved in the impaired subcellular redistribution of PI 3-kinase and the insulin resistance induced by BSO treatment.

The precise mechanism linking NF-κB activation and abnormal subcellular redistribution of PI 3-kinase remains unclear. One possible mechanism of inhibited insulin signalling involves NF-κB-activated transcription of inflammatory cytokines such as TNF-α and interleukin-6. NF-κB plays an important role in regulating inflammatory responses [45, 46] and activation of NF-κB may induce inappropriate inflammatory responses, possibly disrupting insulin signalling. Alternatively, PI 3-kinase activation is reportedly necessary for NF-κB activation [47, 48]. Aberrant NF-κB activation may disrupt the PI 3-kinase pathway via a negative feedback mechanism. An anti-inflammatory agent, salicylate, which stabilises IκB via inhibition of IKK and suppression of NF-κB activation, was shown to restore lipid-induced insulin resistance [49, 50]. Because IKK reportedly induces serine phosphorylation of IRS-1, it is possible that BSO activates IKK, resulting in down-regulation of IRS-1 tyrosine phosphorylation in the LDM fraction and impairment of PI 3-kinase recruitment to the LDM fraction.

In summary, our results suggest that oxidative stress induces insulin resistance by impairing insulin-induced IRS-1 phosphorylation in the LDM fraction and subcellular redistribution of PI 3-kinase, and that NF-κB activation is involved in this process. Our present study provides evidence that the NF-κB pathway plays a role in the pathogenesis of oxidative-stress-induced insulin resistance. Judging from our results and those of previous studies, strategies designed to limit inappropriate activation of NF-κB may be an effective approach to treating insulin resistance.

Acknowledgements. The dominant negative mutant of IκB was kindly provided by Dr Richard Gaynor (University of Texas Southwestern Medical Center at Dallas, Tex., USA). The authors are indebted to Naomasa Kakiya of the University of Tokyo for assistance in various areas of this study.

References

1. Betteridge DJ (2000) What is oxidative stress? Metabolism 49 [Suppl 1]:3–8
2. Reaven GM, Lithell H, Landsberg L (1996) Hypertension and associated metabolic abnormalities—the role of insulin resistance and the sympathoadrenal system. N Engl J Med 334:374–381
3. Tuck ML (1990) Metabolic considerations in hypertension. Am J Hypertens 3:355S–365S
4. Baynes JW (1991) Role of oxidative stress in development of complications in diabetes. Diabetes 40:405–412
5. Paolisso G, D'Amore A, Volpe C et al. (1994) Evidence for a relationship between oxidative stress and insulin action in non-insulin-dependent (type II) diabetic patients. Metabolism 43:1426–1429
6. Jones AF, Winkles JW, Jennings PE et al. (1988) Serum antioxidant activity in diabetes mellitus. Diabetes Res 7:89–92
7. Paolisso G, Di Maro G, Pizza G et al. (1992) Plasma GSH/GSSG affects glucose homeostasis in healthy subjects and non-insulin-dependent diabetics. Am J Physiol 263:E435–E440
8. Paolisso G, Balbi V, Volpe C et al. (1995) Metabolic benefits deriving from chronic vitamin C supplementation in aged non-insulin dependent diabetics. J Am Coll Nutr 14:387–392
9. Paolisso G, Di Maro G, Galzerano D et al. (1994) Pharmacological doses of vitamin E and insulin action in elderly subjects. Am J Clin Nutr 59:1291–1296
10. Rajagopalan S, Kurz S, Munzel T et al. (1996) Angiotensin II-mediated hypertension in the rat increases vascular superoxide production via membrane NADH/NADPH oxidase activation. Contribution to alterations of vasomotor tone. J Clin Invest 97:1916–1923
11. Schnackenberg CG, Wilcox CS (1999) Two-week administration of tempol attenuates both hypertension and renal excretion of 8-Iso prostaglandin f2alpha. Hypertension 33:424–428
12. Ogihara T, Asano T, Ando K et al. (2002) Angiotensin II-induced insulin resistance is associated with enhanced insulin signalling. Hypertension 40:872–879
13. Shimosawa T, Ogihara T, Matsui H et al. (2003) Deficiency of adrenomedullin induces insulin resistance by increasing oxidative stress. Hypertension 41:1080–1085
14. Meister A (1983) Selective modification of glutathione metabolism. Science 220:472–477
15. Khamaisi M, Kavel O, Rosenstock M et al. (2000) Effect of inhibition of glutathione synthesis on insulin action: in vivo and in vitro studies using buthionine sulfoximine. Biochem J 349:579–586
16. Vaziri ND, Wang XQ, Oveisi F, Rad B (2000) Induction of oxidative stress by glutathione depletion causes severe hypertension in normal rats. Hypertension 36:142–146
17. Ogihara T, Asano T, Ando K et al. (2001) Insulin resistance with enhanced insulin signalling in high-salt diet-fed rats. Diabetes 50:573–583
18. Yamamoto Y (1994) Chemiluminescence-based high-performance liquid chromatography assay of lipid hydroperoxides. Methods Enzymol 233:319–324
19. Anderson ME (1985) Determination of glutathione and glutathione disulfide in biological samples. Methods Enzymol 113:548–555
20. James DE, Burleigh KM, Kraegen EW (1986) In vivo glucose metabolism in individual tissues of the rat. Interaction between epinephrine and insulin. J Biol Chem 261:6366–6374
21. Hansen P, Gulve EA, Holloszy JO (1994) Suitability of 2-deoxyglucose for in vitro measurement of glucose transport activity in skeletal muscle. J Appl Physiol 76:979–985
22. Rodbell M (1964) Metabolism of isolated fat cells. I. Effects of hormones on glucose metabolism and lipolysis. J Biol Chem 239:375–380
23. Olefsky JM (1975) Effect of dexamethasone on insulin binding, glucose transport, and glucose oxidation of isolated rat adipocytes. J Clin Invest 56:1499–1508
24. Fujishiro M, Gotoh Y, Katagiri H et al. (2001) MKK6/3 and p38 MAPK pathway activation is not necessary for insulin-induced glucose uptake but regulates glucose transporter expression. J Biol Chem 276:19800–19806
25. Katagiri H, Asano T, Ishihara H et al. (1996) Overexpression of catalytic subunit p110alpha of phosphatidylinositol 3-kinase increases glucose transport activity with translocation of glucose transporters in 3T3-L1 adipocytes. J Biol Chem 271:16987–16990
26. Asano T, Kanda A, Katagiri H et al. (2000) p110beta is up-regulated during differentiation of 3T3-L1 cells and contributes to the highly insulin-responsive glucose transport activity. J Biol Chem 275:17671–17676
27. Satoh S, Nishimura H, Clark AE et al. (1993) Use of bismannose photolabel to elucidate insulin-regulated GLUT4 subcellular trafficking kinetics in rat adipose cells. Evidence that exocytosis is a critical site of hormone action. J Biol Chem 268:17820–17829
28. Anai M, Funaki M, Ogihara T et al. (1998) Altered expression levels and impaired steps in the pathway to phosphatidylinositol 3-kinase activation via insulin receptor substrates 1 and 2 in Zucker fatty rats. Diabetes 47:13–23
29. Sakoda H, Ogihara T, Anai M et al. (1999) No correlation of plasma cell 1 overexpression with insulin resistance in diabetic rats and 3T3-L1 adipocytes. Diabetes 48:1365–1371
30. Anai M, Ono H, Funaki M et al. (1998) Different subcellular distribution and regulation of expression of insulin receptor substrate (IRS)-3 from those of IRS-1 and IRS-2. J Biol Chem 273:29686–29692
31. Kriauciunas KM, Myers MG Jr, Kahn CR (2000) Cellular compartmentalization in insulin action: altered signaling by a lipid-modified IRS-1. Mol Cell Biol 20:6849–6859
32. Lu B, Ennis D, Lai R et al. (2001) Enhanced sensitivity of insulin-resistant adipocytes to vanadate is associated with oxidative stress and decreased reduction of vanadate (+5) to vanadyl (+4). J Biol Chem 276:35589–35598
33. Schreck R, Albermann K, Baeuerle PA (1992) Nuclear factor kappa B: an oxidative stress-responsive transcription factor of eukaryotic cells (a review). Free Radic Res Commun 17:221–237
34. Siebenlist U, Franzoso G, Brown K (1994) Structure, regulation and function of NF-kappa B. Annu Rev Cell Biol 10:405–455
35. Leeuwenburgh C, Ji LL (1995) Glutathione depletion in rested and exercised mice: biochemical consequence and adaptation. Arch Biochem Biophys 316:941–949
36. Czech MP (1995) Molecular actions of insulin on glucose transport. Annu Rev Nutr 15:441–471

37. Saad MJ, Folli F, Kahn JA, Kahn CR (1993) Modulation of insulin receptor, insulin receptor substrate-1, and phosphatidylinositol 3-kinase in liver and muscle of dexamethasone-treated rats. J Clin Invest 92:2065–2072
38. Cusi K, Maezono K, Osman A et al. (2000) Insulin resistance differentially affects the PI 3-kinase- and MAP kinase-mediated signalling in human muscle. J Clin Invest 105:311–320
39. Rudich A, Tirosh A, Potashnik R, Hemi R, Kanety H, Bashan N (1998) Prolonged oxidative stress impairs insulin-induced GLUT4 translocation in 3T3-L1 adipocytes. Diabetes 47:1562–1569
40. Tirosh A, Potashnik R, Bashan N, Rudich A (1999) Oxidative stress disrupts insulin-induced cellular redistribution of insulin receptor substrate-1 and phosphatidylinositol 3-kinase in 3T3-L1 adipocytes. A putative cellular mechanism for impaired protein kinase B activation and GLUT4 translocation. J Biol Chem 274:10595–10602
41. Schreck R, Rieber P, Baeuerle PA (1991) Reactive oxygen intermediates as apparently widely used messengers in the activation of the NF-kappa B transcription factor and HIV-1. EMBO J 10:2247–2258
42. Suzuki YJ, Packer L (1993) Inhibition of NF-kappa B activation by vitamin E derivatives. Biochem Biophys Res Commun 193:277–283
43. Sen CK, Packer L (1996) Antioxidant and redox regulation of gene transcription. FASEB J 10:709–720
44. Yamamoto Y, Gaynor RB (2001) Therapeutic potential of inhibition of the NF-kappaB pathway in the treatment of inflammation and cancer. J Clin Invest 107:135–142
45. Baeuerle PA, Henkel T (1994) Function and activation of NF-kappa B in the immune system. Annu Rev Immunol 12:141–179
46. Barnes PJ, Karin M (1997) Nuclear factor-kappaB: a pivotal transcription factor in chronic inflammatory diseases. N Engl J Med 336:1066–1071
47. Sizemore N, Leung S, Stark GR (1999) Activation of phosphatidylinositol 3-kinase in response to interleukin-1 leads to phosphorylation and activation of the NF-kappaB p65/RelA subunit. Mol Cell Biol 19:4798–4805
48. Reddy SA, Huang JH, Liao WS (2000) Phosphatidylinositol 3-kinase as a mediator of TNF-induced NF-kappa B activation. J Immunol 164:1355–1363
49. Kim JK, Kim YJ, Fillmore JJ et al. (2001) Prevention of fat-induced insulin resistance by salicylate. J Clin Invest 108:437–446
50. Yuan M, Konstantopoulos N, Lee J et al. (2001) Reversal of obesity- and diet-induced insulin resistance with salicylates or targeted disruption of Ikkbeta. Science 293:1673–1677

THE JOURNAL OF BIOLOGICAL CHEMISTRY
Vol. 279, No. 39, Issue of September 24, pp. 41095–41103, 2004
Printed in U.S.A.

Diphtheria Toxin-induced Autophagic Cardiomyocyte Death Plays a Pathogenic Role in Mouse Model of Heart Failure*

Received for publication, December 1, 2003, and in revised form, May 20, 2004
Published, JBC Papers in Press, July 22, 2004, DOI 10.1074/jbc.M313084200

Hiroshi Akazawa‡§, Shinji Komazaki¶, Hiroaki Shimomura‖, Fumio Terasaki‖, Yunzeng Zou‡, Hiroyuki Takano‡, Toshio Nagai‡, and Issei Komuro‡**

From the ‡Department of Cardiovascular Science and Medicine, Chiba University Graduate School of Medicine, 1-8-1 Inohana, Chuo-ku, Chiba 260-8670, Japan, the ¶Department of Anatomy, Saitama Medical School, 38 Morohongou, Moroyama, Iruma 350-0495, Japan, ‖The Third Division, Department of Internal Medicine, Osaka Medical College, 2-7 Daigaku-machi, Takatsuki 569-8686, Japan, and the §Foundation for Biomedical Research and Innovation, 6-1, Minatojima Nakamachi, Chuo-ku, Kobe 650-8543, Japan

It is still not clear whether loss of cardiomyocytes through programmed cell death causes heart failure. To clarify the role of cell death in heart failure, we generated transgenic mice (TG) that express human diphtheria toxin receptor in the hearts. A mosaic expression pattern of the transgene was observed, and the transgene-expressing cardiomyocytes (17.3% of the total cardiomyocytes) were diffusely scattered throughout the ventricles. Intramuscular injection of diphtheria toxin induced complete elimination of the transgene-expressing cardiomyocytes within 7 days, and ~80% of TG showed pathophysiological features characteristic of heart failure and were dead within 14 days. Degenerated cardiomyocytes of the TG heart showed characteristic features indicative of autophagic cell death such as up-regulated lysosomal markers and abundant autophagosomes containing cytosolic organelles like cardiomyocytes of human dilated cardiomyopathy. The heart failure-inducible TG are a useful model for dilated cardiomyopathy, and provided evidence indicating that myocardial cell loss through autophagic cell death plays a causal role in the pathogenesis of heart failure.

Cardiomyocyte death is observed in a number of pathological conditions such as ischemic or dilated cardiomyopathy, hypertensive heart disease, and aging (1). Oncosis has been recognized to be a principal mechanism of myocardial cell death, but during the last decade, much emphasis has been put on the importance of apoptosis on the basis of detectable apoptotic cardiomyocytes in animal and human models of heart failure (2). Recently, autophagic cell death (ACD)[1] has been demonstrated as another type of myocardial cell death in human failing hearts (3–7). Although a decline in pumping capacity initiated by cardiomyocyte loss is supposed to induce ventricular remodeling and finally results in symptomatic heart failure (8), there still remains a controversy over the pathogenic role of cell death in progression of heart failure (9, 10). An intractable problem that hampers mechanistic insights is the low occurrence of myocardial cell death in failing hearts, although it differs strikingly according to the models examined and technical specificity (2, 8). Furthermore, in human hearts, most samples were obtained from patients with end-stage heart failure who underwent heart transplantation and thus it remains unknown whether myocardial cell death occurs persistently from an early stage and is causative to progression of heart failure (8). To circumvent these obstacles, we established an inducible heart failure mouse model utilizing diphtheria toxin (DT)-mediated cell ablation, in which a given number of cardiomyocytes are arbitrarily and synchronously ablated, and prospective and serial analysis is available.

DT is a two-peptide protein consisting of fragments A (DT-A) and B (DT-B) produced by *Corynebacterium diphtheriae* (11). DT binds to the DT receptor on the cell surface through DT-B and is internalized into acidic endocytic vesicles, which allows release of catalytic DT-A into the cytoplasm (12). DT-A exerts its cytotoxicity by ADP-ribosylating elongation factor 2 and thereby inhibiting protein synthesis in infected cells (13). DT receptor has been identified as a precursor of heparin-binding EGF-like growth factor (pro-HB-EGF) (14, 15). Intriguingly, DT cannot bind to rodent pro-HB-EGF because of substitution of amino acids required for DT binding, whereas primate pro-HB-EGF acts as a functional DT receptor (16). Therefore, specific cells in mice are ideally sensitized to DT by forced expression of human pro-HB-EGF (17).

To enable cardiac-specific cell ablation, we generated transgenic mice (TG) expressing human pro-HB-EGF in the hearts under the control of *α-myosin heavy chain* promoter. Administration of DT induced ablation of transgene-expressing cardiomyocytes, and subsequently symptomatic heart failure. In this mouse model of heart failure, autophagy but not apoptosis was the mechanism of cardiomyocyte death. Autophagy is a dynamic process and intracellular constituents are sequestered by membranes and subsequently degradated or recycled in lysosome or vacuole (18–20). In this sense, autophagy is involved in maintaining cellular homeostasis and turnover in physiological conditions. However, a growing body of evidence suggests that autophagy is implicated in execution of pro-

* This work was supported in part by grants from the Japanese Ministry of Education, Science, Sports, and Culture of Japan, Japan Health Sciences Foundation, Takeda Medical Research Foundation, Takeda Science Foundation, Uehara Memorial Foundation, Kato Memorial Trust for Nambyo Research, an the Japan Medical Association (to I. K.) and a Japanese Heart Foundation/Pfizer Japan Grant on Cardiovascular Disease Research (to H. A.), and the New Energy and Industrial Technology Development Organization. The costs of publication of this article were defrayed in part by the payment of page charges. This article must therefore be hereby marked "*advertisement*" in accordance with 18 U.S.C. Section 1734 solely to indicate this fact.

** To whom correspondence should be addressed. Tel.: 81-43-226-2097; Fax: 81-43-226-2557; E mail: komuro-tky@umin.ac.jp.

[1] The abbreviations used are: ACD, autophagic cell death; BNP, brain natriuretic peptide; DT, diphtheria toxin; DT-A, DT fragment A; DT-B, DT fragment B; LAMP-1, lysosome-associated membrane protein-1; MCP-1, macrophage chemoattractant protein-1; MLP, muscle LIM protein; pro-HB-EGF, precursor of heparin-binding epidermal growth factor-like growth factor; SERCA2, sarcoplasmic reticulum calcium-ATPase 2; TG, transgenic mice; WT, wild-type mice.

grammed cell death and is closely linked to several pathological conditions (21–23). Our model of experimentally induced heart failure provided direct evidence that myocardial cell loss through ACD causes heart failure, and will be useful to dissect the molecular mechanisms underlying structural and functional changes in heart failure.

EXPERIMENTAL PROCEDURES

Generation of Transgenic Mice—Human *pro-HB-EGF* cDNA (gift from A. Ullrich, Max-Planck-Institute of Biochemistry, Martinsried, Germany) was subcloned into the α-myosin heavy chain promoter-containing expression vector (gift from J. Robbins, Children's Hospital, Cincinnati, OH). The 6.9-kb DNA fragment was microinjected as a transgene into pronuclei of eggs from BDF1 mice, and the eggs were transferred into the oviducts of pseudopregnant ICR mice. The transgene was identified by Southern blot and PCR analysis. All protocols using mice were approved by the Institutional Animal Care and Use Committee of Chiba University.

Administration of Diphtheria Toxin—Diphtheria toxin (Sigma) was reconstituted in 10 mM sodium phosphate buffer (pH 7.4) containing 5% lactose, and was administered by intramuscular injection.

Northern Blot and in Situ Hybridization Analysis—For Northern blot analysis, total RNA (20 μg) prepared from tissues were hybridized with cDNA probes. Probes for brain natriuretic peptide (*BNP*), skeletal α-actin, sarcoplasmic reticulum calcium-ATPase 2 (*SERCA2*), and *TNF-α* were previously described (24–26). Probes for macrophage chemoattractant protein-1 (*MCP-1*) and collagens (*Col1a2* and *Col3a1*) were gifts from K. Matsushima (Universitty of Tokyo, Tokyo, Japan) and S. Kim (Osaka City University, Osaka, Japan), respectively. Digoxygenin-labeled riboprobes were synthesized by using the 0.7-kb human *pro-HB-EGF* cDNA, and RNA *in situ* hybridization was performed as described previously (27).

Western Blot Analysis—Protein samples were fractionated by SDS-PAGE, and immunoblot analysis was performed as described previously (26, 28).

Transthoracic Echocardiography—Mice were anesthetized by intraperitoneal injection of a mixture of ketamine (100 mg/kg) and xylazine (5 mg/kg). Cardiac function was evaluated with echocardiography (SONOS 4500, Philips, Eindhoven, the Netherlands) using a 12-MHz transducer as described previously (26).

Histological Analysis and Immunohistochemistry—Hearts were fixed in 10% neutralized formalin and embedded in paraffin. Serial sections at 5 μm were routinely stained with hematoxylin-eosin for morphological analysis, and with Masson's trichrome for detection of fibrosis. For measurement of the myocyte cross-sectional area, semithin sections with silver staining were analyzed. Suitable cross-sections were defined as having round-to-oval cardiomyocyte sections and nearly round-shaped capillaries that perfused in the region. For immunohistochemistry, Vectastain ABC kit (Vector Laboratories, Burlingame, CA) was used to detect the primary antibodies. The sections were counterstained with hematoxylin.

Antibodies—The following antibodies were used: goat polyclonal anti-human HB-EGF (R&D Systems, Minneapolis, MN), anti-actin (20–33) IgG fraction of antiserum developed in rabbit (Sigma), mouse monoclonal anti-Ly-6G, mouse monoclonal anti-Mac-3, mouse monoclonal anti-CD3, mouse monoclonal anti-Bcl-xL, mouse monoclonal anti-cytochrome *c* (BD Pharmingen, San Diego, CA), rabbit polyclonal anti-caspase 3, mouse monoclonal anti-phospho-Bad, rabbit polyclonal anti-Bad (Cell Signaling, Beverly, MA), rabbit polyclonal anti-Bcl2, rabbit polyclonal anti-Bax, goat polyclonal anti-cathepsin D, rat monoclonal anti-lysosome-associated membrane protein-1 (LAMP-1), goat polyclonal anti-UBC2, goat polyclonal anti-E6-AP, goat polyclonal anti-UFD1 (Santa Cruz Biotechnology, Santa Cruz, CA), mouse monoclonal anti-COX I (Molecular Probes, Eugene, OR), mouse monoclonal anti-ubiquitin (Chemicon, Temecula, CA), and mouse monoclonal anti-E1 (Upstate, Charlottesville, VA).

Evaluation of DNA Fragmentation—TUNEL assay using paraffin sections was performed with an *in situ* apoptosis detection kit (Takara Biomedicals, Otsu, Japan). For agarose gel electrophoresis for DNA fragmentation, genome DNA (10 μg) was electrophoretically fractionated on a 1.5% agarose gel and stained with ethidium bromide as described previously (29). To induce apoptosis in spleens as positive controls, we injected lipopolysaccharide (40 mg/kg) (Sigma) in phosphate-buffered saline intraperitoneally into age-matched mice. Mice were sacrificed 12 h after lipopolysaccharide injection and spleens were excised (30).

Electronmicroscopy—Hearts were fixed in 3% paraformaldehyde, 2.5% glutaraldehyde, and 0.1 M cacodylate buffer (pH 7.4). After washing with the buffer solution and post-fixation in 1% OsO_4 and 0.1 M cacodylate buffer (pH 7.4), they were washed with the buffer solution, dehydrated using alcohol and acetone, and embedded in epoxy resin. Ultrathin sections were examined under the electron microscope (31).

Statistical Analysis—All values are expressed as mean ± S.E. Comparisons were made by Student's *t* test or one-way analysis of variance as appropriate. Values of $p < 0.05$ were considered statistically significant.

RESULTS

Inducible Myocardial Cell Ablation in TG Expressing Human DT Receptor in the Hearts—To confer DT sensitivity to cardiomyocytes in mice, we generated TG expressing human DT receptor, pro-HB-EGF, under the control of the α-myosin heavy chain promoter (Fig. 1*A*). Of two independent founder lines with successful germline transmission, one line was chosen for further analysis on the basis of transgene expression levels. By immunoblot analysis using an antibody specific for human pro-HB-EGF, we confirmed cardiac-specific expression of the transgene (Fig. 1*B*). *In situ* hybridization analysis using a specific riboprobe for human *pro-HB-EGF* further revealed a mosaic expression pattern of the transgene in the hearts (Fig. 1*C*). Expression of the transgene was scattered throughout the TG hearts, and the number of transgene-expressing cardiomyocytes was 17.3 ± 6.0% out of total cardiomyocytes.

To induce DT-mediated myocardial cell ablation, we administered DT by intramuscular injection to TG and wild-type mice (WT) at 10 weeks of age. When 5 mg/kg DT was administered, TG became lethargic and ~80% of TG died within 10 days after injection of DT, although WT appeared normal (Fig. 1*D*). Immunoblot analysis in combination with *in situ* hybridization analysis revealed that expression of human pro-HB-EGF in the TG hearts was significantly decreased on the next day of DT injection, and almost disappeared on the following day (Fig. 1*E*). After 7 days, transgene-expressing cardiomyocytes were undetected in the TG hearts, suggesting that they were completely ablated through DT-mediated cytotoxicity.

DT-mediated Myocardial Cell Loss Caused Heart Failure in Mice—We next examined the geometric, functional, and histological changes in the hearts caused by DT-mediated myocardial cell damages. Gross inspections of the TG hearts 7 days after DT injection showed global chamber dilatation with marked wall thinning and atrial thrombus (Fig. 2*A*), and the heart to body weight ratios were ~1.3-fold increased (Fig. 2*B*), whereas the mock-treated TG hearts and DT- or mock-treated WT hearts showed no geometric change (Fig. 2).

To evaluate cardiac function, we performed transthoracic echocardiographic examination. Seven days after injection, a ~1.3-fold increase in the left ventricular end-diastolic dimension and a 1.5–1.7-fold decrease in left ventricular wall thickness were observed in DT-treated TG, whereas these parameters were unchanged in mock-treated TG (Fig. 2, *C* and *D*) and DT- or mock-treated WT. Echocardiographic examination also demonstrated a 2.4-fold reduction in % FS in DT-treated TG. These results suggest that injection of DT induced deterioration of LV systolic function with chamber dilatation and ventricular wall thinning in TG. In contrast, no discernible phenotype was observed in TG in the absence of DT, and DT had no harmful effect on WT.

Hematoxylin-eosin staining of the histological sections of TG hearts 7 days after DT injection revealed degenerated cardiomyocytes surrounded by inflammatory cells (Fig. 3*A*). These pathological findings were not observed in WT with or without DT injection (data not shown). The infiltrating inflammatory cells were identified as macrophages by immunohistochemical analysis using anti-Mac-3 antibody (Fig. 3*B*). Histological sections with Masson's trichrome staining showed interstitial fibrosis in DT-treated TG hearts (Fig. 3*A*). Silver staining of the

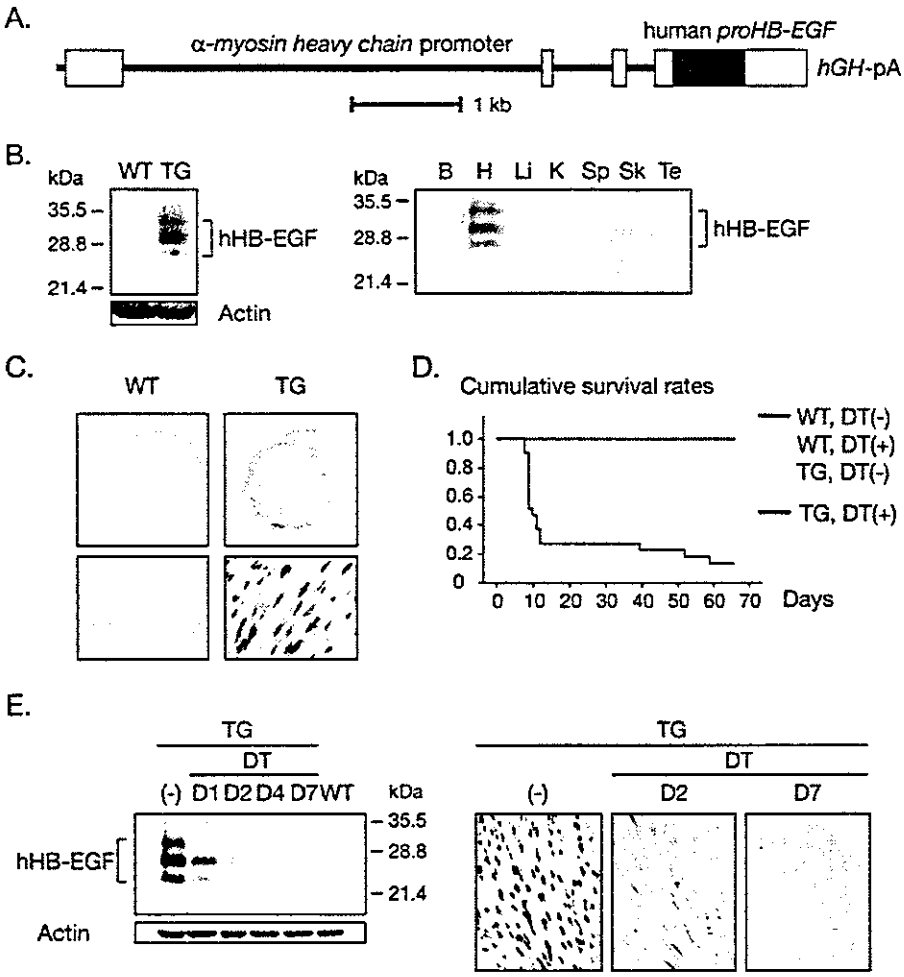

FIG. 1. **DT-induced myocardial cell ablation in transgenic mice expressing human *pro-HB-EGF*.** *A*, schematic representation of the transgene containing α-myosin heavy chain (*αMHC*) promoter, human *pro-HB-EGF* cDNA, and human growth hormone (*GH*) polyadenylation signal (*pA*). *B*, Western blot analysis using an antibody specific for human pro-HB-EGF revealed transgene expression in TG hearts (*left*). Expression of human pro-HB-EGF in TG was observed specifically in the hearts (*right*). *B*, brain; *H*, heart; *Li*, liver; *K*, kidney; *Sp*, spleen; *Sk*, skeletal muscle; *Te*, testis. *C*, *in situ* hybridization analysis using a riboprobe specific for human *pro-HB-EGF*. Transgene was expressed in a mosaic pattern, and cardiomyocytes expressing the transgene were 17.3 ± 6.0% of the total cardiomyocytes within TG hearts. *D*, Kaplan-Meier survival curves of control mice (WT treated with mock or DT and TG treated with mock, $n = 21$, respectively) and TG ($n = 21$) treated with intramuscular injection of DT. *E*, complete ablation of transgene-expressing cardiomyocytes following DT injection revealed by immunoblot (*left*) and *in situ* hybridization analysis. Expression of pro-HB-EGF was remarkably diminished on day 2 (*D2*) and was completely undetected on day 7 (*D7*).

sections of TG hearts on 14 days after DT injection revealed a 1.9-fold increase in cross-sectional areas of cardiomyocytes (Fig. 3*C*), indicating that the cardiomyocytes, which did not express the transgene and survived DT administration, underwent hypertrophic cell growth.

Alterations of Gene Expression in TG Presenting DT-induced Heart Failure—To characterize the molecular basis of heart failure caused by DT-induced myocardial cell ablation, we examined expression levels of several molecular markers. Expression of *BNP* was up-regulated 1 day after DT injection, and persistently elevated thereafter (Fig. 4). Increased expression of skeletal α-actin and decreased expression of *SERCA2* were evident 4 days after DT injection (Fig. 4). Up-regulation of natriuretic peptide genes and fetal cardiac genes including skeletal α-actin is one of the characteristic cellular responses observed during cardiac hypertrophy (32, 33). Especially, ventricular expression of *BNP* is induced promptly in response to volume expansion and pressure overload, and plasma BNP concentrations have proven to be valuable for diagnostic and prognostic assessment in patients with heart failure (34). In addition, down-regulation of *SERCA2* has been reported to be a sensitive marker for heart failure (35). Therefore, these patterns of cardiac gene expression indicated that DT-induced myocardial cell ablation burdened hemodynamic overload and progressed overt heart failure concomitantly with cardiac hypertrophy.

Consistent with the histological finding of infiltration by macrophages, an increase in expression of *MCP-1* was observed 1 day after DT injection, and expression levels of *MCP-1* were further increased until 4 days and declined on 7 days (Fig. 4). The expression levels of *TNF-α*, encoding an inflammatory cytokine produced by macrophages, changed in parallel with that of *MCP-1* (Fig. 4). Insomuch as symptomatic heart failure was evident 7 days after DT injection, stressed myocardium could be another source of *TNF-α* production at this period. Following up-regulation of inflammatory markers, expression levels of the collagen genes (*Col1a2* and *Col3a1*) were increased at 4 days after DT injection (Fig. 4). These temporal profiles of

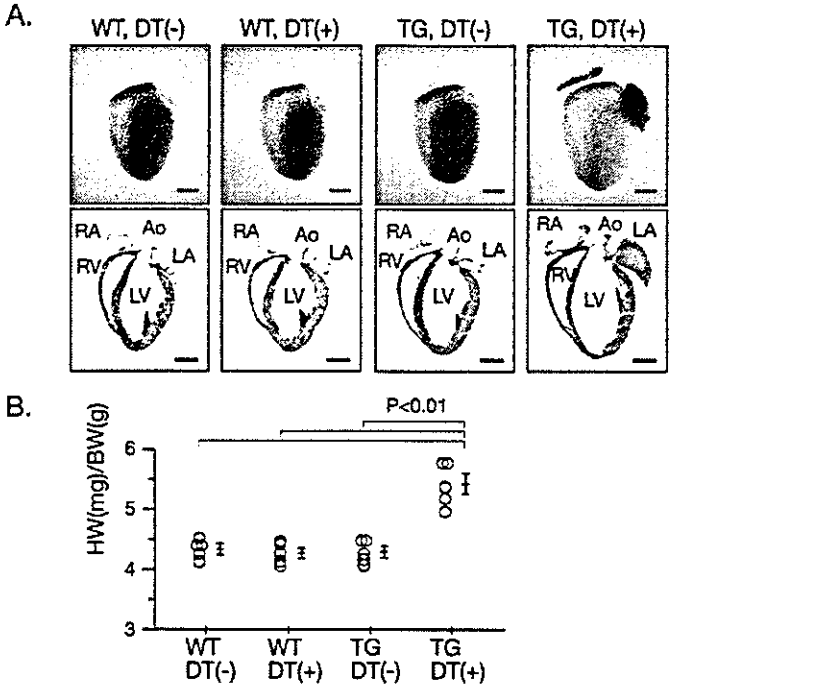

D.

	WT, DT(-)	WT, DT(+)	TG, DT(-)	TG, DT(+)
Number	10	10	10	10
Age (weeks)	10.7±0.4	10.6±0.5	11.5±0.3	10.9±0.3
BW(g)	24.0±1.7	24.1±1.2	24.8±0.4	24.3±1.3
HR (beats/min.)	261.0±15.9	258.9±18.8	256.3±18.4	252.3±18.0
LVDd (mm)	3.69±0.14	3.71±0.17	3.75±0.23	4.69±0.71
LVDs (mm)	2.05±0.13	2.11±0.20	2.08±0.27	3.81±0.46
FS (%)	44.2±4.7	43.2±4.9	47.4±3.5	19.4±3.0
IVSth (mm)	0.65±0.03	0.65±0.03	0.66±0.02	0.45±0.03
LVPWth (mm)	0.65±0.03	0.66±0.02	0.66±0.02	0.39±0.03

FIG. 2. **DT-induced cardiomyocyte loss caused heart failure in mice.** *A*, gross morphology of whole hearts (*upper rows*) and longitudinal sections (*lower rows*) of WT and TG 7 days after DT or mock injection. *Ao*, aorta; *LA*, left atrium; *LV*, left ventricle; *RA*, right atrium; *RV*, right ventricle. *Bar*, 2 mm. *B*, increase in heart to body weight ratios observed in TG 7 days after DT injection. *C*, representative M-mode echocardiograms. *IVS*, interventricular septum; *LVPW*, left ventricular posterior wall. *D*, echocardiographic measurements. *BW*, body weight; *FS*, fractional shortening; *HR*, heart rate; *IVSth*, interventricular thickness in end-diastole; *LVDd*, left ventricular diameter in end-diastole; *LVDs*, left ventricular diameter in end-systole; *LVPWth*, left ventricular posterior wall thickness in end-diastole.

gene expressions suggest that mobilization of macrophages are induced by up-regulated MCP-1 after the myocardial cell ablation, leading to cardiac fibrosis by enhanced production of inflammatory cytokines, and that inflammatory cytokines and cardiac remodeling might promote left ventricular dysfunction evoked by myocardial cell loss.

Myocardial Cell Death Induced by DT Is Not Primarily because of Apoptosis—To investigate the mechanisms of myocardial cell death in DT-treated TG hearts, we first performed a TUNEL assay. In the hearts of DT-treated TG, we could not detect any TUNEL-positive cardiomyocytes or inflammatory cells, whereas a marked increase in TUNEL-positive cells was detected in the spleen of mice treated with intraperitoneal administration of lipopolysaccharide as positive controls (Fig. 5*A*). Likewise, analysis of genomic DNA by agarose gel provided no evidence of DNA laddering in DT-treated TG hearts (Fig. 5*B*). We further examined activation of caspase 3 (Fig. 5*C*), changes in expression of proapoptotic and antiapoptotic Bcl2 family proteins (Fig. 5*D*), and cytochrome *c* release from mitochondria (Fig. 5*E*), but biochemi-

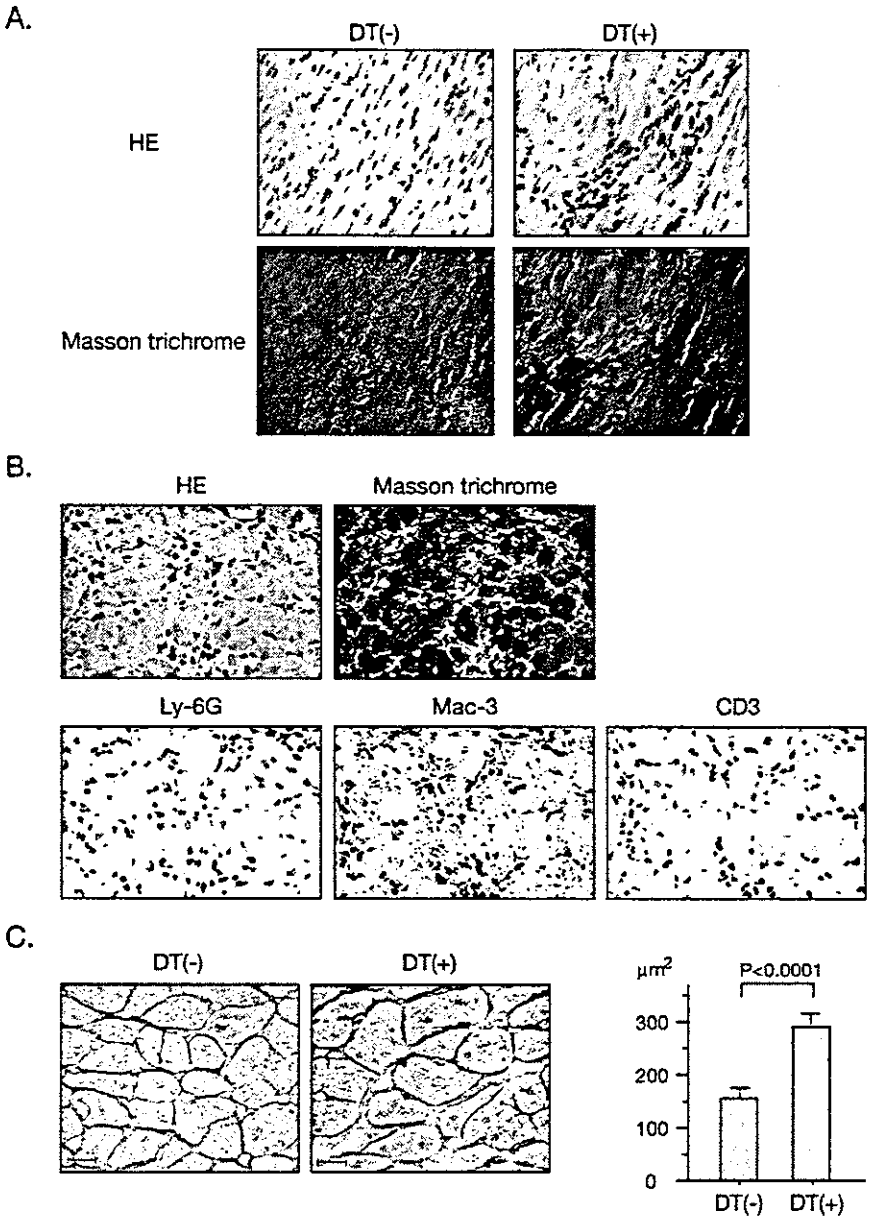

FIG. 3. **Histological analysis of the hearts after DT injection.** *A*, serial sections with hematoxylin-eosin (*HE*) staining revealed cardiomyocyte degeneration and infiltration of inflammatory cells 7 days after DT injection. Masson's trichrome staining showed interstitial fibrosis. *B*, infiltrating inflammatory cells were predominantly macrophages with positive staining for Mac-3 but not for Ly-6G nor CD3. *C*, silver staining of TG hearts 14 days after DT injection revealed an increase in the cross-sectional area of cardiomyocytes, indicating hypertrophic compensation of myocardial cells without transgene expression.

cal changes leading to typical apoptosis were not observed in DT-treated TG hearts.

Autophagy Is the Mechanism of Myocardial Cell Death in DT-induced Failing Hearts—ACD is a regulated process of caspase-independent programmed cell death, in which intracellular components are degradated by lysosomal or proteasomal proteases (21–23). Immunohistochemical analysis revealed positive staining for lysosomal protease cathepsin D, LAMP-1, and ubiquitin in cardiomyocytes of DT-treated TG hearts (Fig. 6*A*). It is notable that cathepsin D showed a diffuse cytosolic distribution, whereas LAMP-1 showed a granular localization. These results suggest an increase in formation of lysosomes and leakage of activated lysosomal enzymes into the cytosol. Recently, it has been reported that, in human failing hearts, ubiquitin accumulation in cardiomyocytes may be associated with up-regulation of ubiquitin-conjugating enzyme E2 (UBC2) and down-regulation of deubiquitinating enzymes such as UFD1 and isopeptidase T (6). However, Western blot analysis revealed that the amounts of the ubiquitin-activating enzyme E1, UBC2, ubiquitin-ligating enzyme E3 (E6-AP), and UFD1 were not unchanged in DT-treated TG hearts when compared with control hearts (Fig. 6*B*).

Electron microscopic analysis revealed abundant cytosolic vacuoles and segmented configuration of nuclei with lumpy con-

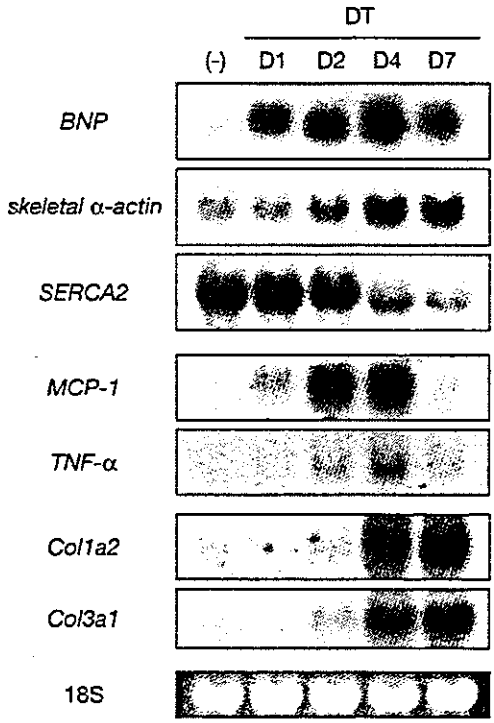

FIG. 4. **Alterations in gene expression after DT injection.** Temporal profiling of gene expression following administration of DT (5 mg/kg). Expression levels of cardiac genes, inflammatory cytokine genes, and collagen genes were examined by Northern blot analysis.

densation of chromatin in degenerated cardiomyocytes in TG hearts 3 days after DT injection (Fig. 7, *A* and *B*). However, nuclear fragmentation and crescent-shaped chromatin condensation at the nuclear periphery typical of apoptosis were not observed. In higher magnifications, cytosolic vacuoles containing lipid droplets with myelin figures and degenerated mitochondria (Fig. 7, *C* and *D*), suggested that these vacuoles are typical autophagosomes. In terminally degenerated cardiomyocytes, lysis of myofibrills and other intracellular organelles were prominent (Fig. 7*E*). These findings suggest that myocardial cell loss in DT-treated TG hearts is primarily because of ACD.

Autophagic degeneration has been implicated in human failing heart failure (3–7). We also found cardiomyocytes undergoing autophagic cell death in a biopsied specimen from a 43-year-old patient suffering from dilated cardiomyopathy. Similar to the electron micrographic findings in degenerated cardiomyocytes in our mouse model of heart failure, myofibrillar degeneration in association with cytosolic vacuoles and lipid droplets were observed in this biopsied specimen (Fig. 7*F*). The vacuoles were autophagosomes containing digested organelles. These findings are illustrative of the previously reported features characteristic of ACD in human heart failure. Therefore, degenerated cardiomyocytes in human dilated cardiomyopathy patients showed ultrastructural alterations similar to those in our mouse model of heart failure.

DISCUSSION

In this study, we generated a novel mouse model of heart failure, where cardiomyocyte loss through ACD is arbitrarily and specifically induced by intramuscular injection of DT. Recent technical progress in genetic manipulation and physiological measurements enabled us to produce several mouse models of heart failure (36). These models have improved our understanding of pathophysiology of heart failure and have been of great help for establishment and evaluation of new therapeutic approaches. Genetically engineered mice, in particular, expanded the list of gene products that are involved in generation or progression of heart failure, but they have specific limitations as animal models. For example, mice homozygous for muscle LIM protein (*MLP*) develop cardiomyopathy and heart failure, but the clinical courses of individual mice are divergent because the penetrance of phenotype is influenced by genetic backgrounds (37). About half of the *MLP*-deficient mice suffer from severe congestive heart failure and die during the second postnatal week, but the rest of the *MLP*-deficient mice survive to adulthood and are viable. Development of cardiomyopathy is also identified in tropomodulin-overexpressing transgenic mice (38). In this model, severe signs of heart failure are observed between 2 and 4 weeks after birth and most symptomatic mice die within a few days. The phenotypes of these model mice are primarily genotype-dependent, but are susceptible to the effects of genetic backgrounds. In addition, a difficulty in morphological and biochemical approach in studying a role of cardiomyocyte death in heart failure arises from the low occurrence of cell death in these models (2). In our mouse model of heart failure, cardiomyocytes expressing the DT receptor are selectively and simultaneously damaged by administration of DT, and this advantageous feature not only makes it possible to induce symptomatic heart failure arbitrarily but also provides insights into the roles of cell death in heart failure.

Our model appears conceptually similar to the one reported in the earlier work (39), in which DT-A expression is regulated by a tetracycline-responsive promoter. In that model, induction of DT-A in the hearts resulted in congestive heart failure as well. However, a leaky induction is occasionally observed in this tetracycline-inducible system, and subtle expression of DT-A might have nonspecific and undesirable effects, insomuch as the toxicity of DT-A is extremely high (17). In our model, the DT receptor, not injurious in the absence of DT, was expressed in the hearts, and myocardial cell ablation was specifically and ideally achieved.

Temporal histological analysis and profiling of gene expression revealed a series of cellular events that finally evoked heart failure (Figs. 3 and 4). Transgene expression was dramatically reduced in a few days after DT injection (Fig. 1*E*), suggesting that cardiomyocyte death occurs during that period. Following cardiomyocyte death, inflammatory cells infiltrated and produced inflammatory cytokines. Around 7 days, hemodynamic deterioration with apparent cardiac remodeling induced symptomatic heart failure. These findings strongly suggest that myocardial cell death causes symptomatic heart failure. In addition, our model allowed quantitative analysis of cardiomyocyte death. *In situ* hybridization analysis revealed that expression of the transgene was scattered diffusely and observed in 17.3 ± 6.0% of cardiomyocytes in TG hearts. Because there was no cardiomyocyte expressing the transgene on day 7 after DT injection, all of the transgene-expressing cells (~17% of cardiomyocytes) might be dead. These results suggest that loss of this population is sufficient to produce symptomatic heart failure, and this estimation is consistent with the notion that a diffuse loss of 10–20% of cardiomyocytes accounts for cardiac failure, whereas equivalent cardiac failure is produced by a segmental loss of 40–50% of cardiomyocytes after coronary artery occlusion (40).

Electron microscopic analysis revealed that, in our mouse model, damaged cardiomyocytes showed abundant cytoplasmic autophagosomes and chromatin condensation with more complex and lumpier shapes than in apoptosis, both of which are characteristic of ACD (Fig. 7). ACD is defined as a regulated pathway of cytoplasmic degradation executed by lysosomal and